Zr_{54}-Al_{17}-Co_{29}-Nb_x(X=0.5wt%1wt%)非晶質金屬玻璃合金銲接性影響之研究

[1]吳紹齊[1]吳柏樟

指導教授：[1*]王惠森 、陳厚光

[1]義守大學材料科學與工程學系

科技部計畫編號:MOST108-2221-E-214-018-

Introduction

1. 在生物相容性考量下，不含 Cu 和 Ni 生醫用途的 ZrCoAl 塊狀金屬玻璃(Bulk Metallic Glass, BMG)合金，其具備有傳統 Zr-Cu 基 BMG 優異的高強度、高硬度、耐磨耗以及耐蝕性佳等優越的性質。
2. 但在韌性、延展性及塑性變形程度上表現 較差，為了改善此一種缺點，在此合金系統內嘗試添加具有改善延展性與韌性的 Nb，但這會使 ZrCoAl BMG 原本較 低的玻璃形成能力(Glass-Forming Ability, GFA)或熱穩定性進一步地降低，因此對此類合金系統的銲接形成 一大挑戰。
3. 本研究將針對添加 Nb 之 ZrCoAl BMG 合金，以 Nd:YAG 雷射銲接的方式，配合銲接參數和液體冷卻裝置組合進行銲接實驗，並在完成銲接之工作，經由各種分析後，了解 Nb 添加其對銲接後銲道及熱影響區之微觀組織和機械性質及腐蝕等方面之影響。

關鍵詞：塊狀金屬玻璃(BMG)，銲接，玻璃形成能力(GFA)，微組織，機械性質，耐蝕性

Experimental Processes

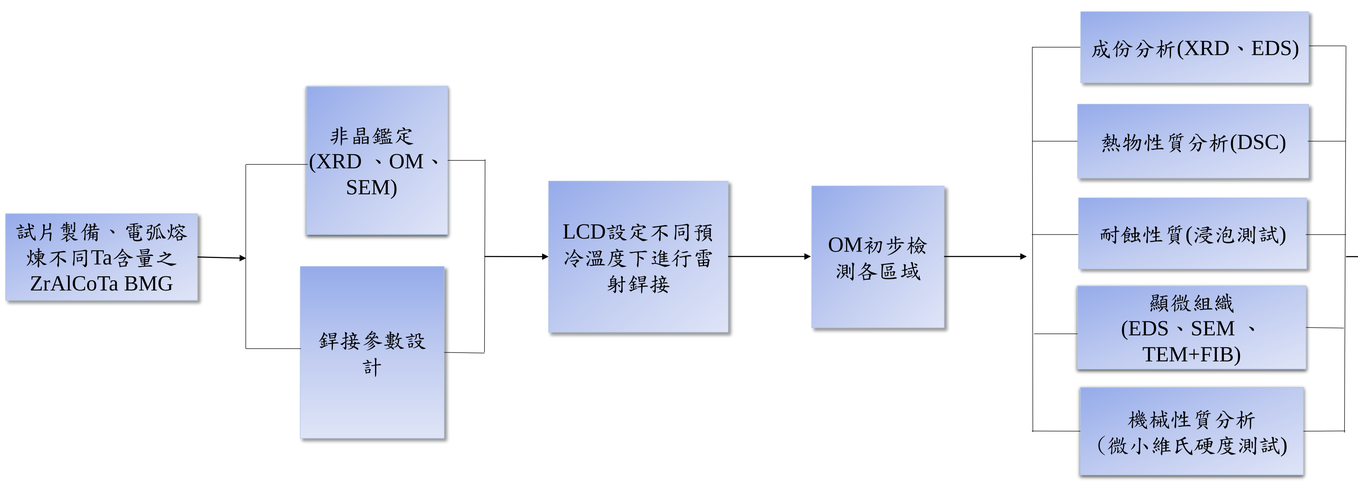

(a)結晶結構(b)非晶結構示意圖

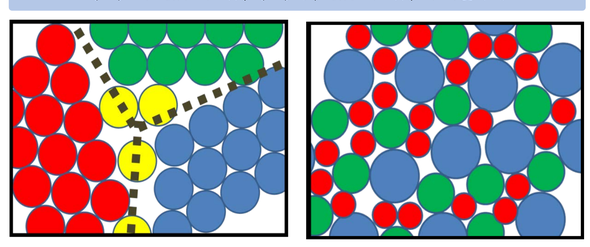

非晶質合金是指原子間以短程有序或是無序的方式排列

Results and Discussion

銲接參數設計

	Laser voltage	Peak power	Pulse Frequency	Pulse duration	Laser energy	Spot size	Gas flow rate
A	238	1.3	2.0	4.6	6.0J	0.4	10
B	243	1.4	2.0	4.6	6.5J	0.4	10
C	249	1.5	2.0	4.6	7.0J	0.4	10

母材銲前觀察

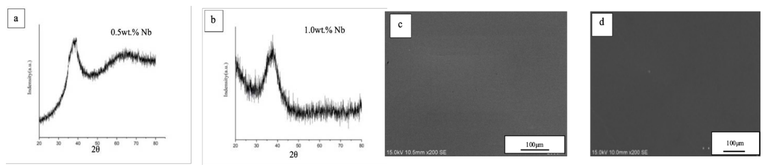

鑄件母材觀察XRD (a) 0.5 wt% Nb (b) 1.0 wt% Nb SEM觀察 (c) 0.5 wt% Nb (d) 1.0 wt% Nb

不同銲接起始溫度 OM 橫截面觀察

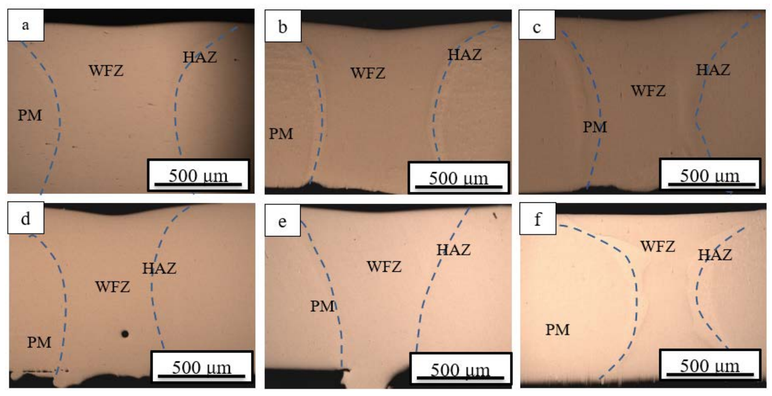

在銲道及熱影響區中並無觀察到明顯缺陷產生

不同銲接起始溫度 SEM 微組織觀察

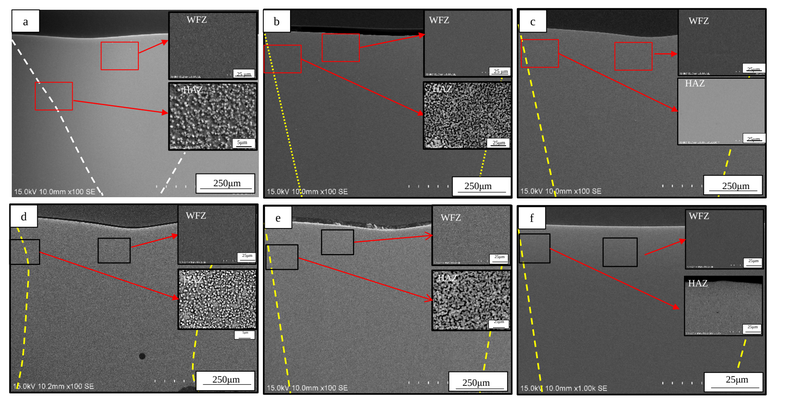

1、於IWT 0 ˚C銲結時，在銲道及熱影響區中較不會產生結晶
2、於IWT 10 ˚C及RT銲接時，可以在WFZ中觀察到明顯的結晶區
3、在銲道中皆無明顯的結晶產生

室溫下銲接之 HAZ TEM 結晶相鑑定

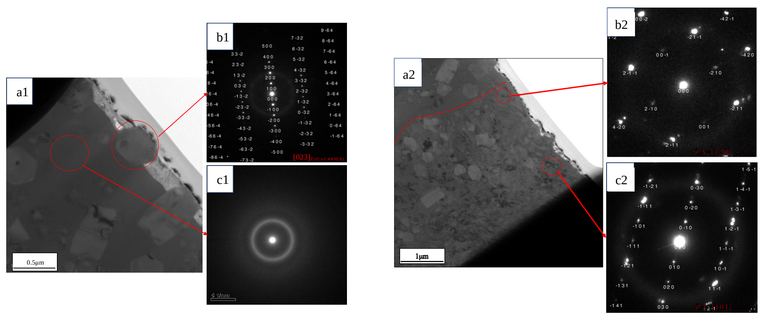

由鑑定結果可以得知當中有大尺寸結晶相被鑑定為具有六方晶結構Zr_6CoAl_2相小尺寸結晶相被鑑定為$Zr(Co_{1.4}Al_{0.6})$相

0 ºC 銲接之 WFZ及HAZ TEM 觀察結果

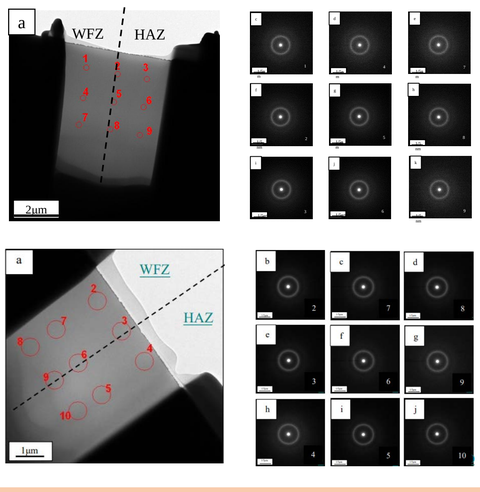

不管是在WFZ或HAZ，甚至WFZ及HAZ的交界處皆在擇區繞射中顯示當預冷溫度降低至0℃時，以上所述區域皆呈現非晶環

室溫及其他初始銲接溫度銲後浸泡腐蝕後之SEM觀察

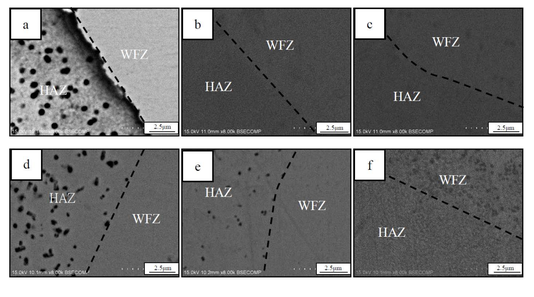

在WFZ位置幾乎沒有觀察到孔蝕的產生，WFZ在雷射銲接後能保持非晶結構，因此有更好的抗腐蝕能力

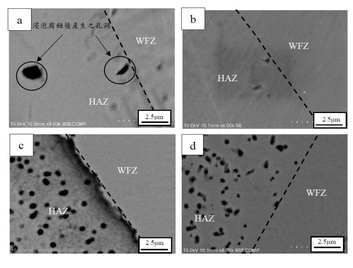

在不同預冷溫度銲接後浸泡測試3及5天表面孔蝕分布情形結果顯示，HAZ產生之結晶相腐蝕對銲件耐蝕性有重大影響

銲接熱循環曲線計算

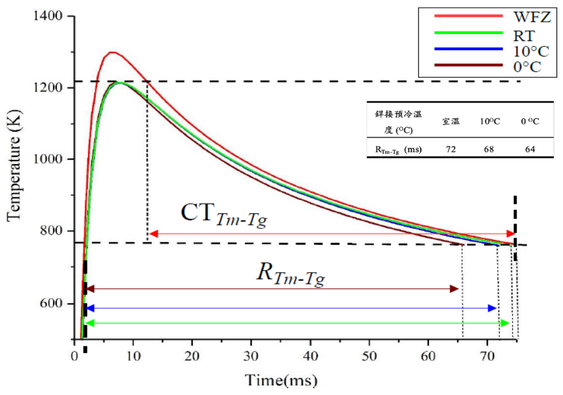

冷卻的停留時間RTm / Tg差異非常微小，隨著預冷溫度降低而降低。為避免 BMG經雷射銲接後在HAZ中產生結晶，銲接熱循環中Tm與Tg之間加熱至冷卻的停留時間RTm / Tg應低於64毫秒。

母材及不同銲接起始溫度之 DSC 結果

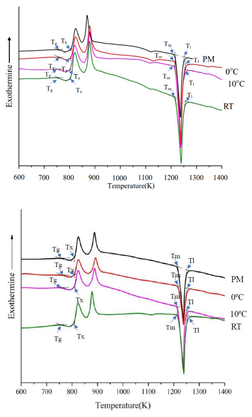

IWT	T_g	T_x	ΔT_x	T_m	T_l	γ	γ_m
PM	752	803	51	1216	1247	0.403	0.685
0℃	752	802	50	1214	1247	0.401	0.683
10℃	757	803	46	1213	1248	0.400	0.680
RT	754	800	46	1214	1246	0.400	0.679

IWT	T_g	T_x	ΔT_x	T_m	T_l	γ	γ_m
PM	761	811	50	1216	1247	0.403	0.685
0℃	760	810	50	1214	1247	0.401	0.683
10℃	763	810	47	1213	1248	0.400	0.680
RT	765	810	45	1214	1246	0.400	0.679

DSC曲線無太大差別，預冷溫度降低，結晶相隨著預冷溫度降低而減少，使GFA指數中的ΔT_x獲得一定的改善，使得ΔT_x回復至與母材相當。

母材及不同銲接起始溫度之硬度比較結果

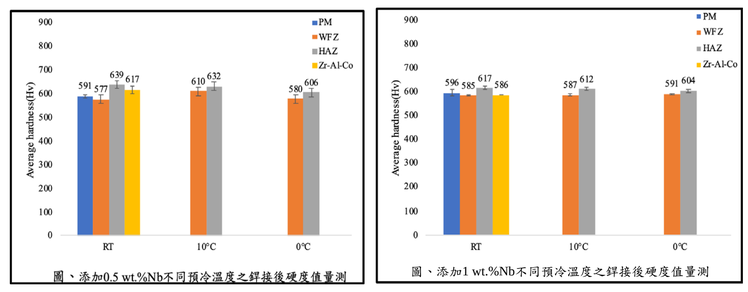

圖、添加0.5 wt.%Nb不同預冷溫度之銲接後硬度值量測

圖、添加1 wt.%Nb不同預冷溫度之銲接後硬度值量測

室溫下雷射銲接後，銲道與母材之硬度差異不大，熱影響區產生兩種不同的結晶相造就了不同的影響，當預冷溫度降低至0 ºC時其熱影響區與母材硬度差異不大

Conclusions

- 室溫下雷射銲接後，發現$Zr_{54}Al_{17}Co_{29}Nb_x$ BMG之WFZ仍保持非晶結構，但在HAZ中發現兩種不同結構之結晶相，經TEM相鑑定分析後，分別為大尺寸六方晶結構的Zr_6CoAl_2相和小尺寸的$Zr(Co_{1.4}Al_{0.6})$相。
- 在預冷溫度為0 ℃雷射銲接後，經TEM檢測可以知道為非晶結構，透過HAZ之銲接熱循環曲線的觀察，發現如未避免使$Zr_{54}Al_{17}Co_{29}Nb_X$ BMG雷射銲接後HAZ中發生結晶行為，$R_{Tm\ /\ Tg}$應低於64毫秒，因此擁有較佳的HAZ耐蝕特性。
- 銲後$Zr_{54}Al_{17}Co_{29}Nb_x$ (x=0.5 wt.% or 1.0 wt.%) BMG 之GFA相近，因此其熱物性質、機械性質、耐蝕性差異不大。

以各類纖維及固體潤滑劑製作環保無銅磨擦材料製程及性質研究

學生:安倬均、楊凌竹、劉冠汝、洪沂鈴、盧嬿晴、邱欣儀、楊采芳、張輔元　　指導教授:李國榮

研究動機與目的

非石棉有機磨擦材料 (Non Asbestos Organic, NAO)為目前商用煞車材料最常使用的磨擦材料之一，其中，在磨擦材料中的**銅原料**具有易塑性變形、優良的機械性質及極佳的導熱性，因此銅有穩定磨擦係數、增加磨擦材料強度、減少熱衰退的用途。但近年來發現銅會危害水生生物，其中環境中大部分的銅微粒源自煞車的磨屑，有導致鮭魚迷失洄游方向及不孕等狀況，美國已制定法案於2025年將磨擦材料中的**銅含量**限制在0.5%以下，因此開發環保無銅磨擦材料為未來重要的發展方向；**硫化銻**為層狀結構材料，具有潤滑性、可穩定磨擦係數的作用，但有部分研究指出其會於制動過程因高溫而轉化成對人有害的有毒物質，因此取代硫化銻能成為一項對環境及人體健康之友善目標。

因此本研究探討以來取代無銅NAO磨擦材料中銅的成分磨擦材料中的銅原料將被限制，以及硫化銻對人體有潛在的致癌性，以陶瓷纖維(水鎂石纖維、矽灰石纖維)取代磨擦材料中的銅纖維作為強化材，及以鐵粉取代銅粉；層狀結構原料(雲母、焦炭)取代硫化銻作為固體潤滑劑，再以鐵纖維取代銅纖維及以鐵粉取代銅粉，對無銅磨擦材料的磨潤、磨耗、熱傳、機械性質的影響，並評估其應用在煞車用途上的可行性。

實驗方法

試片代號及成分配比表(Vol%)

成分 / 代號	銅纖維	鐵纖維	銅粉	鐵粉	水鎂石纖維	矽酸鹽纖維	硫化銻	雲母	焦炭	其他
NAO	2.55	1.16	2.55	0	-	-	1.95	-	-	91.79
NCuO	0	1.22	0	0	-	-	2.06	-	-	96.72
BF	0	0	0	2.55	2.55	-	1.95	-	-	91.79
WF	0	0	0	2.55	-	2.55	1.95	-	-	91.79
MiCa	0	3.71	0	2.55	-	-	-	1.95	-	91.79
Coke	0	3.71	0	2.55	-	-	-	-	1.95	91.79

其他：酚醛樹脂、芳綸纖維、鈦酸鉀纖維、鋼絲絨、鋁粉、二氧化鋯、二氧化矽、石墨、碳化矽、Cashew、硫酸鋇、硫化銻、NBR。

甩罐機

V型混粉機

油壓機

熱壓模具

高溫爐

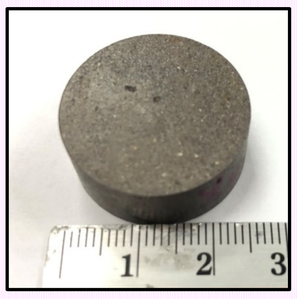

磨擦材料
(直徑2.54 cm，厚度1 cm)

實驗流程圖

洛氏硬度機

熱傳導分析儀

自組式磨耗試驗機

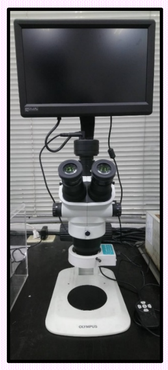

光學顯微鏡

結果與討論

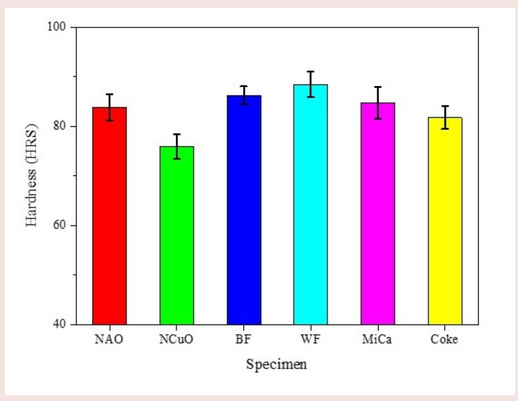

各類試片硬度值

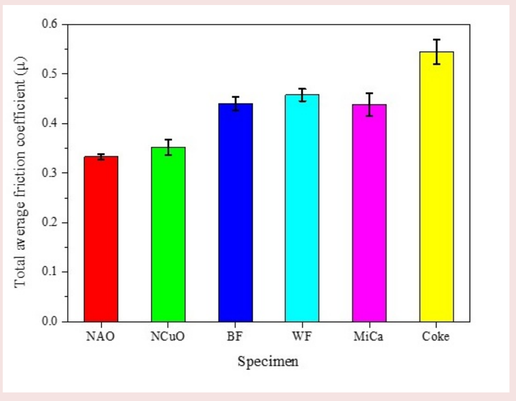

各類試片總磨擦係數

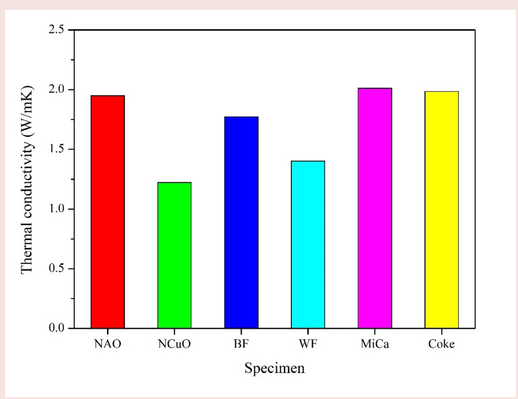

各類試片熱傳導係數

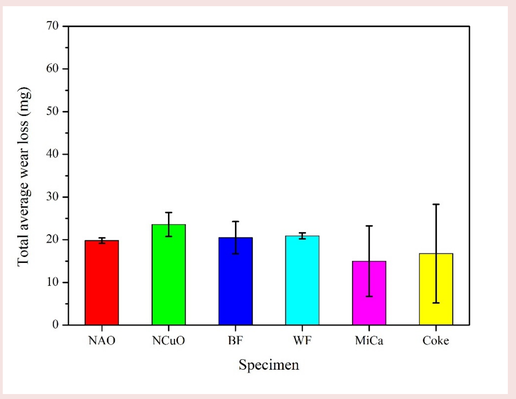

各類試片總磨耗量

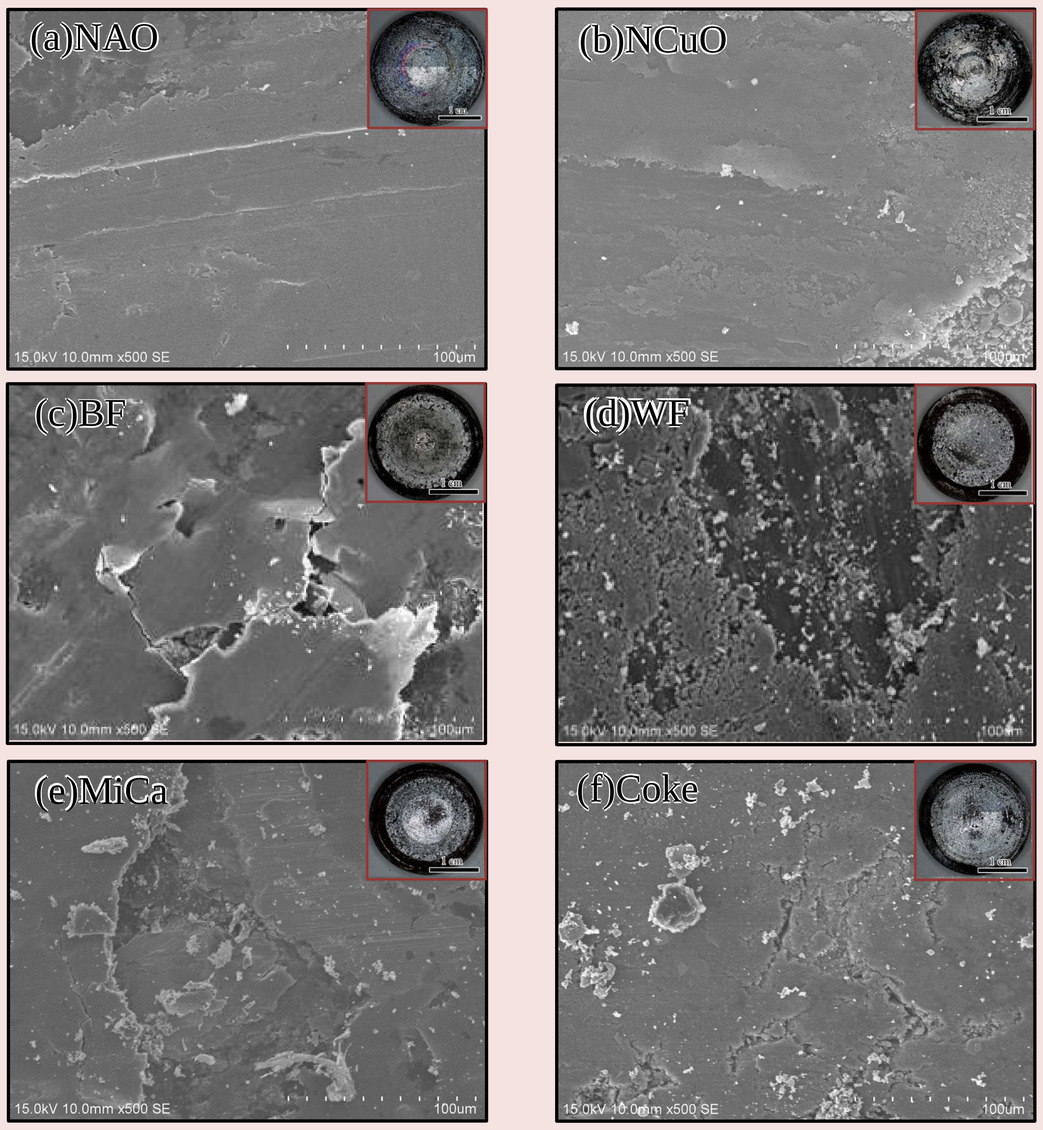

各類試片磨耗面外觀圖與SEM顯微組織

結論

- 焦炭的添加能提升材料的磨擦係數，且磨耗量減少有利於延長材料的使用壽命。
- 雲母的添加能提升試片的熱傳導係數，能減少熱衰退的情形發生，但在磨擦係數方面表現稍低。
- 矽灰石的添加能提升硬度值、磨擦係數，但在熱傳導及磨耗量方面較差。
- 添加焦炭及矽灰石之環保無銅磨擦材料試片，具有良好磨擦係數及磨擦穩定性，且磨耗量較低，因此這兩種材料是具有潛力的。

致謝

在此由衷感謝義守大學貴儀中心及金屬中心提供量測設備與儀器，以及大詠城機械提供原料贊助(鑄鐵)，使本研究得以順利進行各項實驗，僅此致謝。

以抽氣過濾及旋鍍改質製備巴克紙應用於電化學生物感測器之探討

陳雨函、潘沛緹、蔡沂霖、*李國榮、薛安婷、蕭子柔、許高維

義守大學材料科學與工程學系

摘 要

本研究採用羧化前後之奈米碳管以抽氣過濾法製成巴克紙感測器試片，利用羧化方式使奈米碳管擁有較多的羧基官能團，並提高表面活性及親水性，接著旋鍍上EDC/NHS改質劑於羧化巴克紙感測器試片，以提升巴克紙試片的親水性，再添加不同濃度的牛血清白蛋白後觀察電化學變化的趨勢，最後將巴克紙感測器試片放置於冰箱及乾燥箱兩種環境不同時間之放置實驗，藉此評估其作為癌症篩檢應用的可行性。實驗結果顯示，羧化後之奈米碳管能夠增加巴克紙感測器試片的親水性質，並提升與蛋白質接合的能力，在EDC/NHS改質後的試片添加不同濃度之牛血清白蛋白後，其電化學性質也有明顯變化，而試片接合蛋白質後其試片檢測系統不會因為不同環境及時間的放置實驗下喪失其檢測效能。

實驗步驟

奈米碳管 → CNT羧化與否

添加分散劑

研磨

超音波震盪

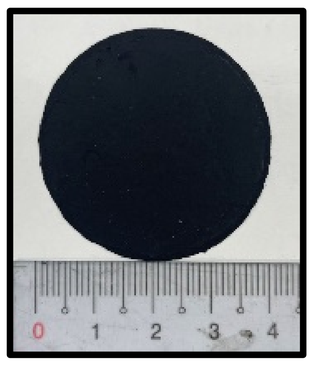

過濾抽氣成型

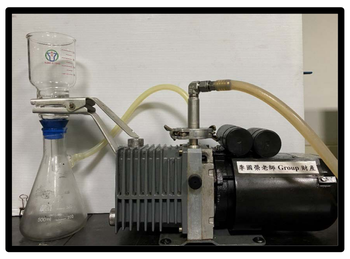

烘箱烘乾

巴克紙試片

旋鍍劑改質

接觸角量測

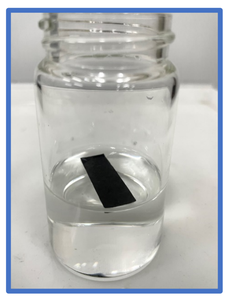

牛血清白蛋白添加

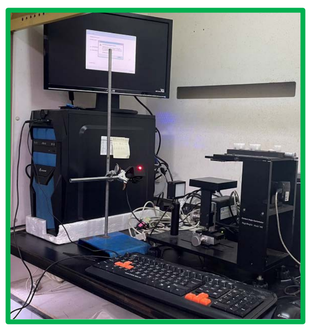

性質量測

電化學性質量測

顯微組織觀察

放置時間實驗

電化學性質量測

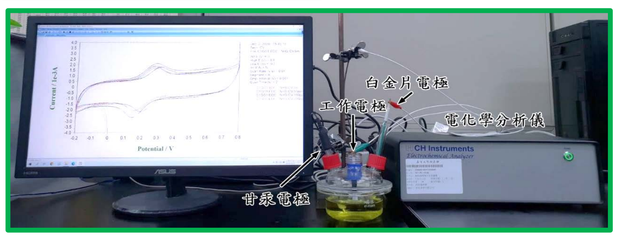

實驗流程圖

實驗結果

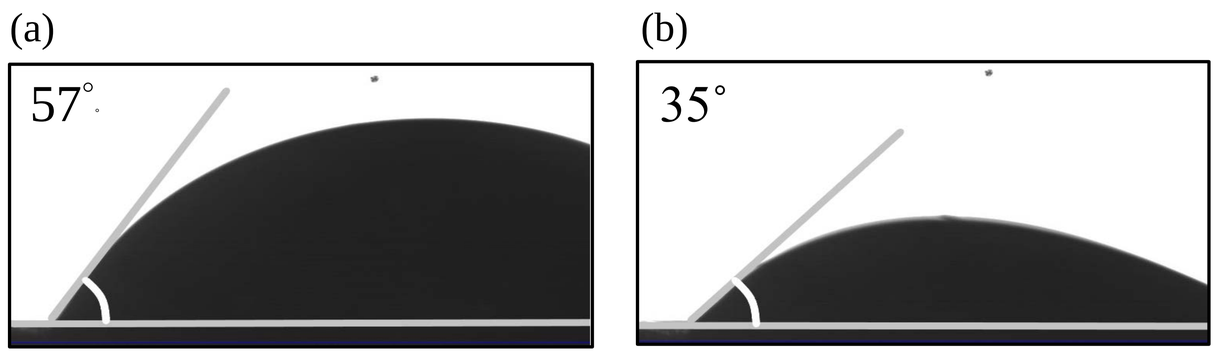

羧化奈米碳管前後之接觸角(a) 未羧化57°(b) 羧化35°

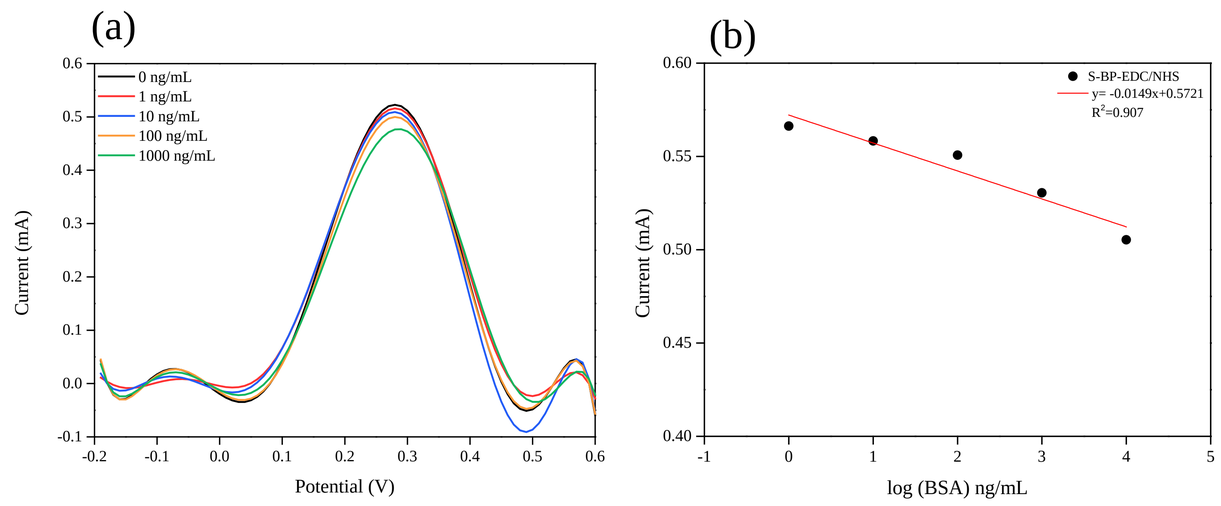

S-BP-EDC/NHS試片(a)添加不同濃度蛋白質後之電化學性質比較(b)添加不同濃度蛋白質後之線性回歸分析

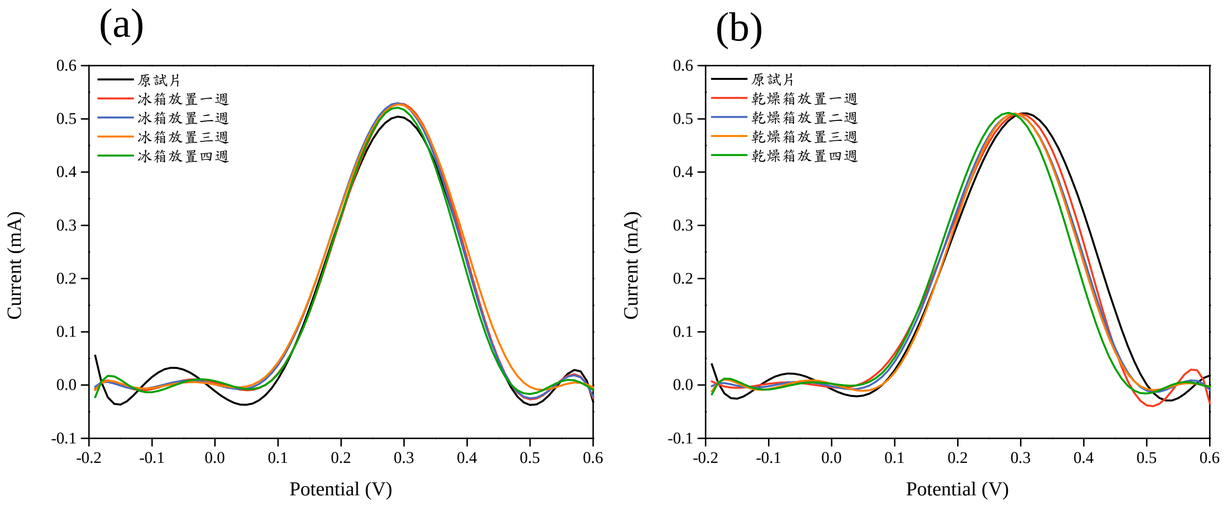

S-BP-EDC/NHS試片添加牛血清白蛋白於不同放置時間及環境實驗(a)放置於冰箱(b)放置於乾燥箱

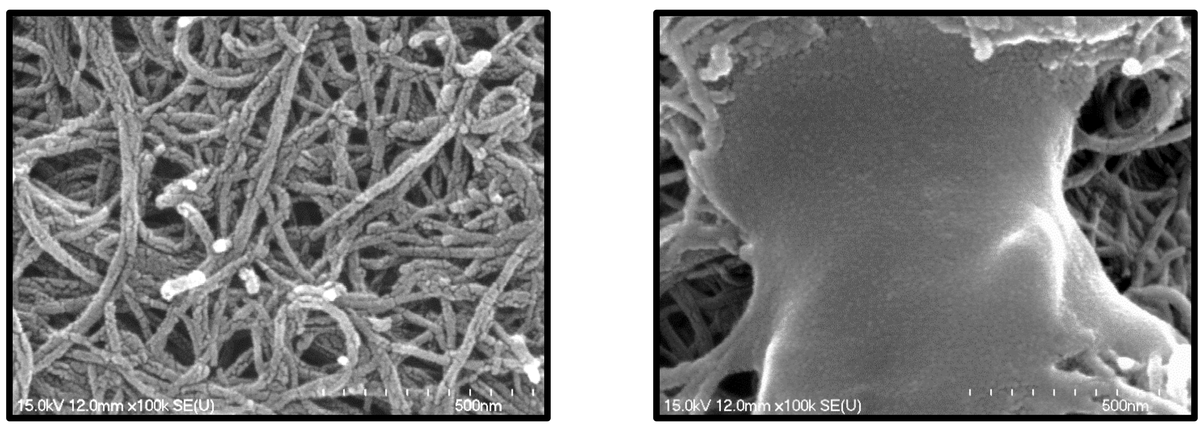

S-BP 試片添加蛋白質前後的顯微結構比較

結 論

1. 在兩種巴克紙感測器試片(BP、S-BP)中，在接觸角量測中顯示由羧化奈米碳管製成之巴克紙感測器試片親水性最佳。
2. 試片經過EDC/NHS改質後添加不同濃度之牛血清白蛋白，其試片電化學之氧化電流值會隨著蛋白質濃度增加而呈現線性關係，顯示改質後對於蛋白質濃度變化的靈敏度提升。
3. 試片於不同放置時間在冰箱及乾燥箱內，接合蛋白質後其檢測系統不會因為不同環境及時間的放置實驗下喪失其檢測效能。

致 謝

本研究承蒙義守大學暨義大醫院經費補助(計畫編號：ISU-106-IUC-04)，及共同主持人－義大醫院心臟內科王朝平博士；也感謝科技部經費補助(計畫編號: MOST 109-2221-E-214-020、MOST 110-2221-E-214-003)；使本研究得以順利進行，謹此致謝。

碳/活化製程對酚醛樹脂混合三嵌段共聚物含浸美耐皿海綿所製備的多孔碳電極影響之探討

王瑄圻 許心怡 顏世卿 王浚宇 *李國榮 鄭鉅齊 陳品安 廖育婕 陳宥穎 張晏維
義守大學材料科學與工程學系

摘 要

本研究使用美耐皿海綿(Ms)作為載體，並含浸至由酚醛樹脂(P)混合三嵌段共聚物(F)的前驅體含浸液內，接著將經由穩定化後的美耐皿海綿試片進行碳化、活化劑KOH活化製程，即可製得具有大孔、中孔及微孔的塊狀多孔碳材，再將其作為超級電容器的碳電極使用之研究，探討不同的碳化溫度(600℃、800℃、1000℃)製程會使製備出的塊狀多孔碳材在電化學性質及顯微結構變化，最後將電化學性質表現最好的試片進行活化劑KOH活化，製得塊狀多孔碳材試片，並對其進行表面特性分析與電化學性質量測。

關鍵字：超級電容器、美耐皿海綿、酚醛樹脂、三嵌段共聚物、活化劑KOH、多孔碳電極、電化學、比電容值

實驗方法

美耐皿海綿 → 含浸液配製 --- 酚醛樹脂 / 三嵌段共聚物 / 無水酒精

→ 恆溫攪拌 --- 40 ℃，10 min

→ 真空攪拌含浸 --- 20 kPa，160 rpm，10 min

→ 穩定化 --- 180 ℃，12 hr

→ 碳化 --- 800 ℃，2 hr

→ 活化 --- 塊材：KOH = 1：1，800 ℃，1.5 hr

→ 酸洗 --- 0.5 M 硫酸

→ 酸鹼中和

→ 烘乾 --- 100 ℃，12 hr

→ 塊狀多孔碳材試片

→ 表面特性分析 → SEM、BET

→ 電化學性質量測 → CV、Cp、EIS、循環壽命

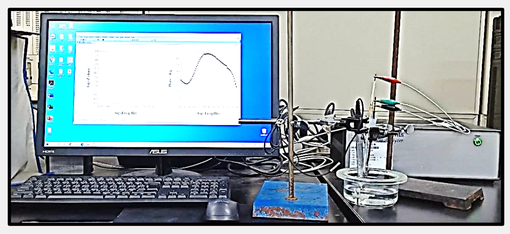

各類經不同碳化溫度製程試片之電化學性質表

試片代號	CV比電容值 (F/g)	充放電時間 (s)	電荷轉移電阻 (ohm)	擴散參數
Ms-P1F1-600-**C**	18.08±2.33	2.33	4.596	1.327
Ms-P1F1-800-**C**	31.83±2.61	35.04	2.250	1.924
Ms-P1F1-1000-**C**	22.41±1.52	29.17	4.890	2.641

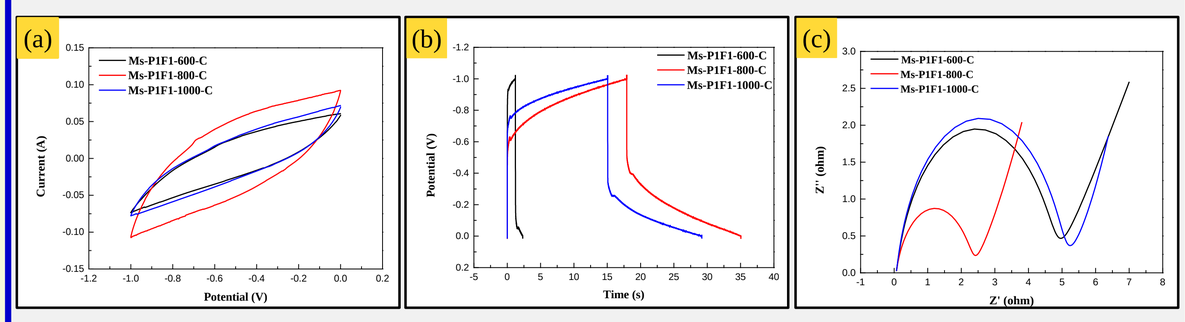

各類經不同碳化溫度製程試片之電化學量測，(a) CV圖、(b) Cp圖、(c) EIS圖

活化前後試片之BET分析表

試片代號	比表面積 (m^2/g)	孔體積 (cm^3/g)	微孔含量 (%)	中孔含量 (%)
Ms-P1F1-800-**C**	215.90	0.57	0	100
Ms-P1F1-800-**CA**	801.51	0.86	46.46	48.52

活化前後試片之電化學性質表

試片代號	CV比電容值 (F/g)	充放電時間 (s)	電荷轉移電阻 (ohm)	擴散參數	電容保持率 (%)
Ms-P1F1-800-**C**	31.83±2.61	35.04	2.250	1.924	104 %
Ms-P1F1-800-**CA**	40.32±12.73	87.81	3.303	1.936	111 %

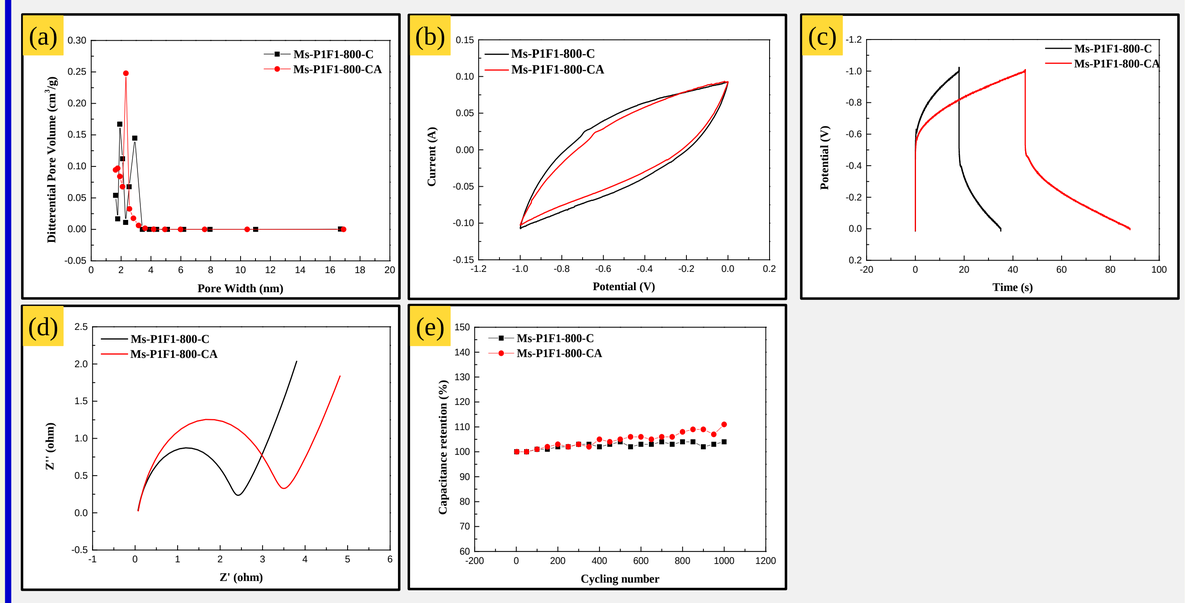

活化前後試片之BET分析與電化學量測，
(a) 孔徑分佈圖、(b) CV圖、(c) Cp圖、(d) EIS圖、(e) 循環壽命圖

結果與討論

Ms與Ms-P1F1試片分別在600℃、800℃、1000℃之不同碳化溫度下的250 x、50k x顯微結構表

試片 / 倍率	Ms	Ms-P1F1-600-**C**	Ms-P1F1-800-**C**	Ms-P1F1-1000-**C**
250 x	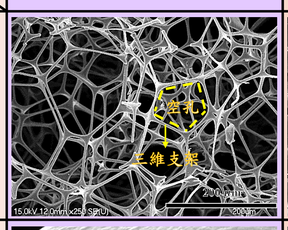	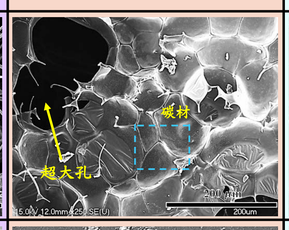	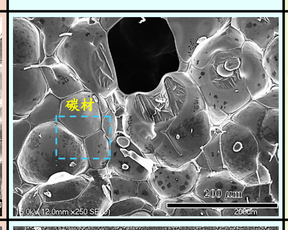	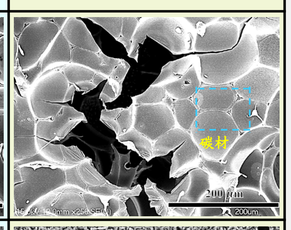
50k x	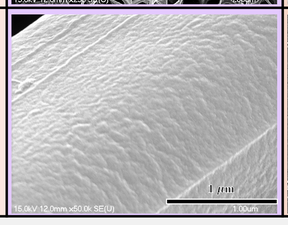		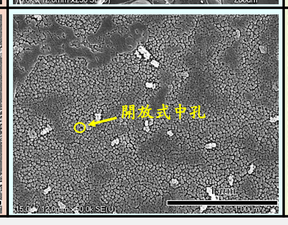	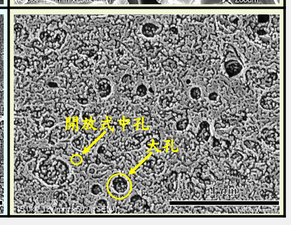

Ms-P1F1-800試片之活化前後的250 x、50k x顯微結構表

試片 / 倍率	Ms-P1F1-800-**C**	Ms-P1F1-800-**CA**
250 x	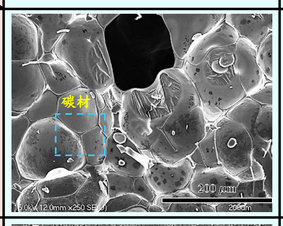	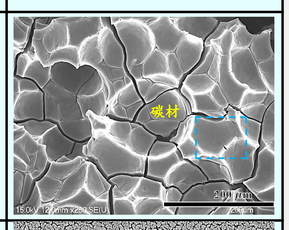
50k x	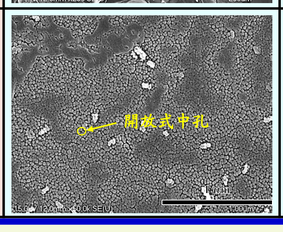	

結 論

Ⅰ. 碳化溫度的影響

1. 碳化溫度在800℃時的Ms-P1F1-800-C試片有較好的CV比電容值(31.83±2.61 F/g)、Cp比電容值(28.31±1.82 F/g)、較長充放電時間(35.04 s)及較小的電荷轉移電阻值(2.25 ohm)，因此選擇其進行後續的活化製程。

Ⅱ. 活化前後製程的影響

1. 活化後試片有較高的比表面積(801.51 m^2/g)、孔體積(0.86 cm^3/g)；且可知活化前試片有中孔結構，活化後試片有微孔及中孔結構。
2. 活化後試片有較好的CV比電容值(40.32±12.73 F/g)、Cp比電容值(42.76±8.74 F/g)、較長充放電時間(87.81 s)、較大的擴散參數(1.936)、良好的電容保持率(111 %)。

致 謝

本研究承蒙科技部計畫(MOST 108-2221-E-214-015)及(MOST 109-2221-E-214-020)、義守大學貴儀中心的支持，研究得以順利進行，謹此致謝。

利用常壓化學氣相沉積製程成長功能性氧化物及二維材料之研究

陳厚光*，陳熙玲，劉玟欣，陳家宏，洪子宸，王怡涓，陳澔霖
義守大學-材料科學與工程學系
*Corresponding Author：houguang@isu.edu.tw

摘要

- 為了發展全氧化物電子元件，p-n介面是基礎，因此需要有適合且良好的p、n型材料。過去實驗室使用藍寶石基板成長平坦的n型氧化鋅膜層已成功生長，本次實驗使用雲母作為可撓式基板，希望能夠成功使其應用在可撓式元件上，本次實驗摻雜目的是希望提升薄膜的性能，期望薄膜表面電性良好。
- 透明導電薄膜有n型跟p型兩種，其中n型發展大多已經成熟，然而p型發展卻較為緩慢。主要是p型薄膜，電性表現較差，不易成長。本實驗採用的氧化鎳是典型的p型透明氧化物薄膜，透過n型跟p型的結合，可以應用在薄膜電晶體和發光二極體 。
- 近年來，二維材料的興起，過渡金屬二硫族化物(TMDCs)具有半導體的特性，其中二硫化鉬也為此類，為了將二硫化鉬薄膜應用在光偵測元件，我們需要大面積且均勻的薄膜，透過改變前驅物的參數，實現具有高品質及厚度均勻的薄膜。

實驗流程

- 霧化化學氣相沉積(Mist-CVD)

酸洗實驗所使用到器具，放入載台、將所有零件裝好，設定溫度600度(每分鐘3℃升溫速率)，持溫一小時，倒入前驅物溶液，開啟氣瓶和流量控制器並設定流速為2SLM，開始震盪，震盪結束空冷降溫，取出試片、清洗器具。

- 常壓化學氣相沉積法(APCVD)

通氬氣，將石英管內的真空狀態變成常壓狀態後，放入載台，開機使腔體升溫，升溫速率12℃/min，製程溫度為750度，硫的溫度持溫210度，待至製程結束後降溫取出試片。

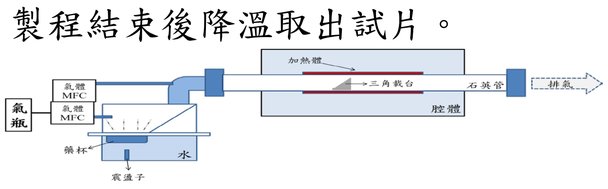

圖 1 Mist-CVD實驗裝置示意圖

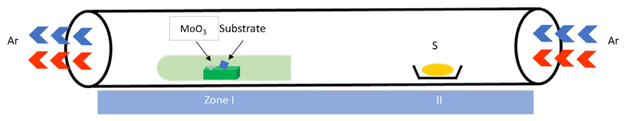

圖 2 APCVD實驗裝置示意圖

表面形貌及微結構分析

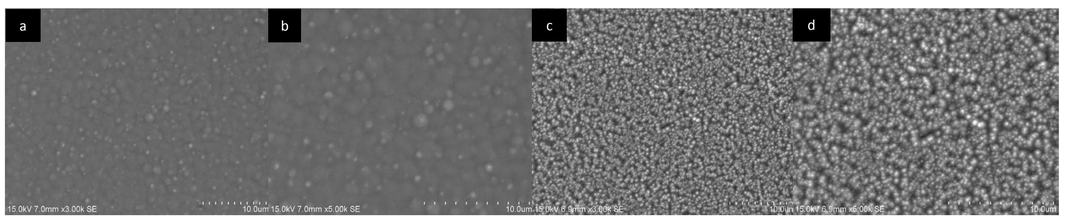

圖 3 Mist-CVD生長氧化鋅薄膜摻雜Ga的SEM圖像(a)1.5mM 倍率30k(b)1.5mM 倍率50k(c)3.0mM 倍率30k(d)3.0mM 倍率50k

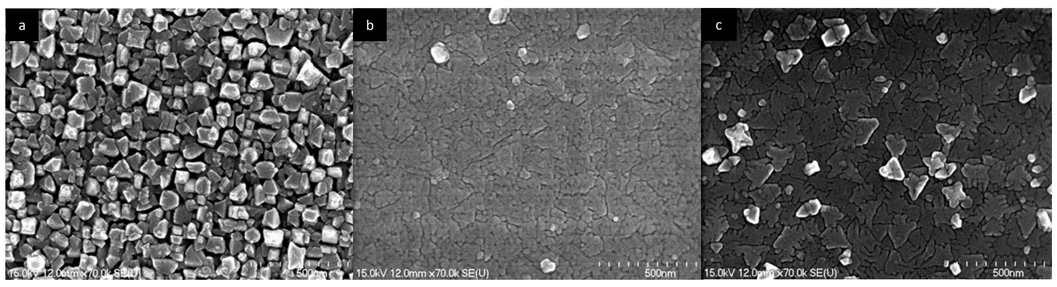

圖 4 Mist-CVD生長氧化鎳薄膜在不同基板上的倍率70k的SEM圖像(a)未退火雲母(b)退火c-plane藍寶石(c)退火a-plane藍寶石

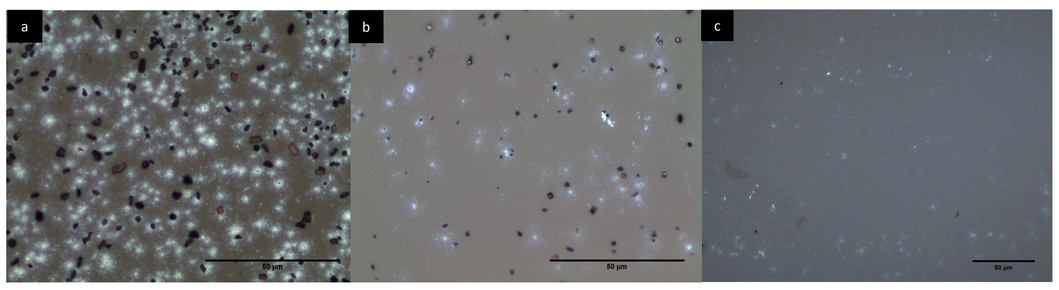

圖 5 APCVD生長二硫化鉬薄膜使用不同前驅物量的OM圖像(a)7 mg (b)5 mg(c)4 mg

結論

1. 氧化鋅晶粒沿著c軸優選方位生長，而鎵的摻雜會使晶粒變小。透過XPS檢測證明鎵離子成功固溶至氧化鋅的晶格中。霍爾量測電學性質分析，退火後不同濃度之試片載子濃度提高、電阻值降低，證明微量的鎵摻雜和退火可以幫助膜層表面導電性變佳。透過UV穿透光譜可以得知較高濃度的鎵摻雜使其透明度較差。
2. 成功透過Mist-CVD在a-plane、c-plane藍寶石及雲母基板上生長氧化鎳薄膜，其中以c-plane藍寶石最為光滑。由UV穿透光譜顯示，在各個基板上生長的氧化鎳均具有高透光率。透過霍爾量測得知通過鋰摻雜能改善載子濃度及電阻率。
3. 拉曼光譜圖顯示生長的薄膜是二硫化鉬且為單層的薄膜，透過PL圖可以得知生長的薄膜具有高品質，使用不同量的前驅物比對，目前4 mg的前驅物量可以長出膜層均勻度且癒合度高的薄膜。

XPS

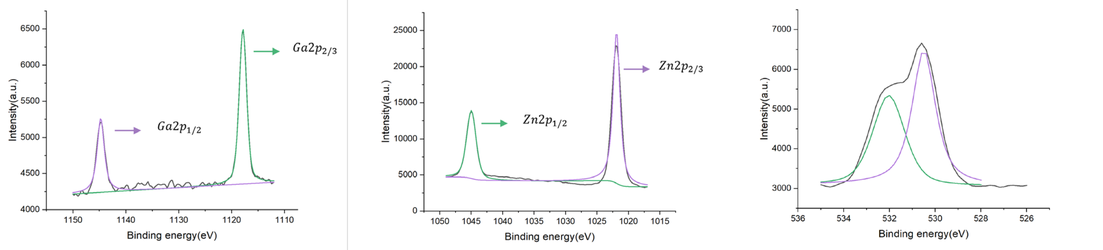

圖 6 氧化鋅薄膜摻雜1.5mM Ga

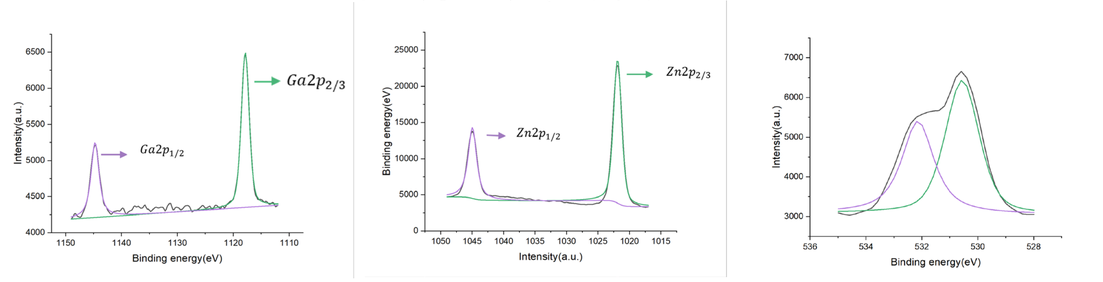

圖 7 氧化鋅薄膜摻雜3.0mM Ga

UV穿透光譜

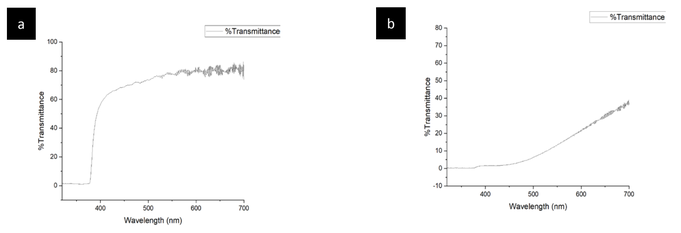

圖 8 氧化鋅薄膜摻雜Ga(a)1.5mM(b)3.0mM

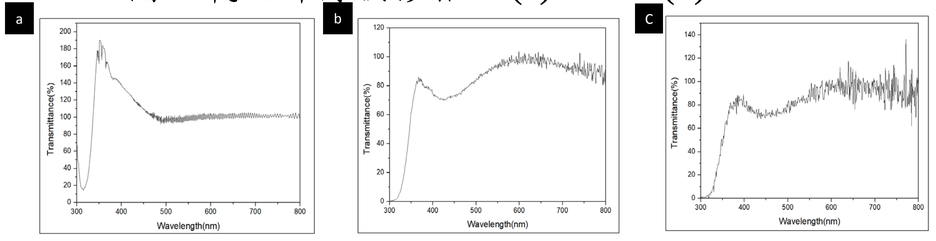

圖 9 氧化鎳薄膜在(a)未退火雲母(b)退火c-plane藍寶石(c)退火a-plane藍寶石

霍爾量測

基板	摻雜濃度	mobility(cm2/Vs)	Resistivity(Ohm-cm)	carrier concerntration(cm-3)	type
未摻雜	0	2.99	4.43	2.70×10^{17}	n
未摻雜退火	0	24.90	1.91×10^{-2}	4.36×10^{18}	n
1.5mM	1.5mM Ga	13.69	1.69×10^{-1}	6.03×10^{17}	n
1.5mM退火	1.5mM Ga	7.97	1.45×10^{-3}	5.79×10^{19}	n
3.0mM	3.0mM Ga	14.57	2.07×10^{-1}	5.06×10^{18}	n
3.0mM退火	3.0mM Ga	5.15	2.59×10^{-2}	4.04×10^{20}	n

圖 10 氧化鋅薄膜生長在雲母基板上不同條件的霍爾量測圖

基板	Resistivity(Ohm-m)	Bulk concentration(m-3)	type
退火A面藍寶石 (未參雜Li)	1.81E+03	5.16E+14	p
退火A面藍寶石 (參雜Li)	2.80E+03	1.09E+14	p

圖 11 氧化鎳薄膜生長在不同基板上的霍爾量測圖

拉曼及PL分析

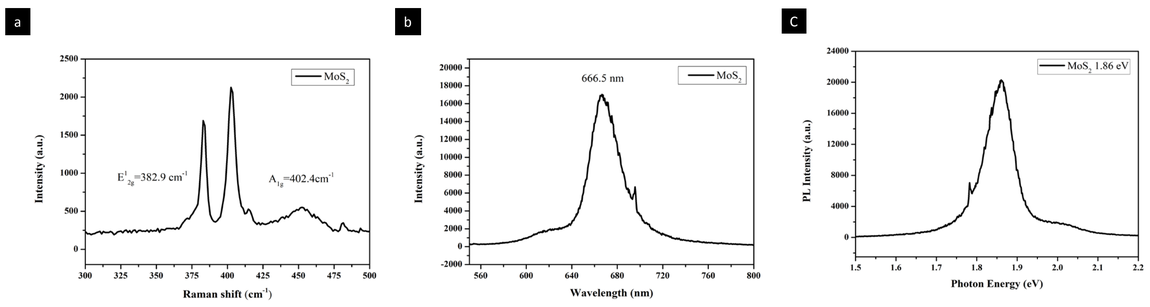

圖 12 二硫化鉬薄膜的(a)拉曼光譜圖(b)PL光譜(c)能隙圖

Research on the properties of p-type and n-type thin films materials for transparent optoelectronic devices

Pei-Ci Yang, Chih-Chuan Fu, Yong-Shun Huang, Bo-Wei Huang, Bing-Chen Hou, Zhi-Hong Jian, Sheng-Hong Wang, You-Xuan Hu, Yung-Hui Shih, Guo-ju Chen**

Department of Materials Science and Engineering,I-SHOU University

Abstract

Transparent conducting oxides (TCO) are electrical conductive materials with comparably low absorption of electromagnetic waves within the visible region of the spectrum. They are usually prepared with thin film technologies and used in opto-electrical apparatus such as solar cells, displays, opto-electrical interfaces and circuitries[1]. TCO films have a light transmittance of more than 80%, energy gap of above 3.1eV as well resistivity is lower than 10^{-3} Ω-cm. The most famous applied material in n-type TCO films is Indium Tin Oxides (ITO), visible light transmittance is above 85%, resistivity is lower than 10^{-3} Ω-cm[2]. And Cu_2O which can grow at a low temperature is a good p-type semiconductor, which energy gap of about 2.17eV.

ITO films (n-type)

Experimental

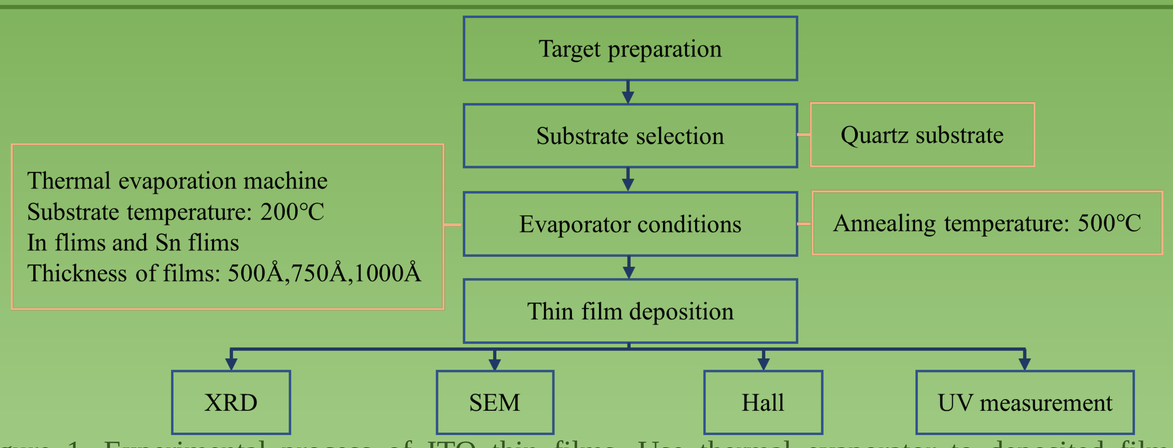

Figure 1. Experimental process of ITO thin films. Use thermal evaporator to deposited films thickness 500Å,750Å,1000Å on quartz glass, then atmospheric annealing at 500˚C for 3hours.

Results and Discussion

XRD

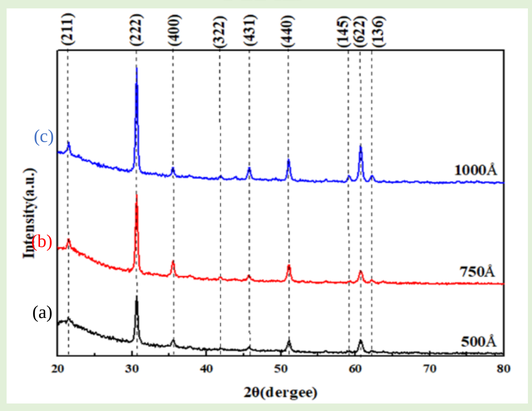

Figure 2.XRD patterns of the film with different thickness: (a)500Å, (b)750Å and (c)1000Å.

Optical property

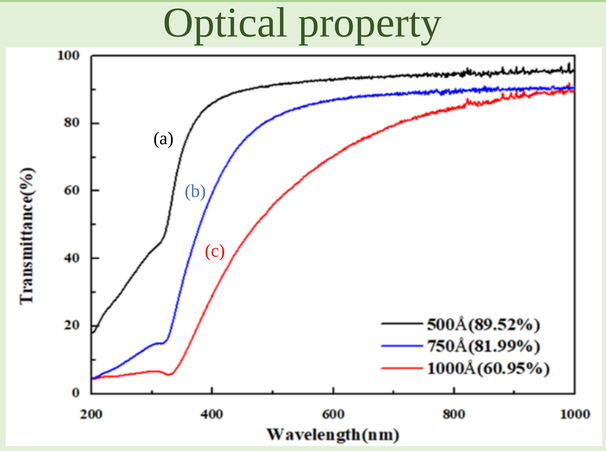

Figure 3. Transmittance of the different film thickness: (a)500Å, (b)750Å and (c)1000Å.

Hall Measurement

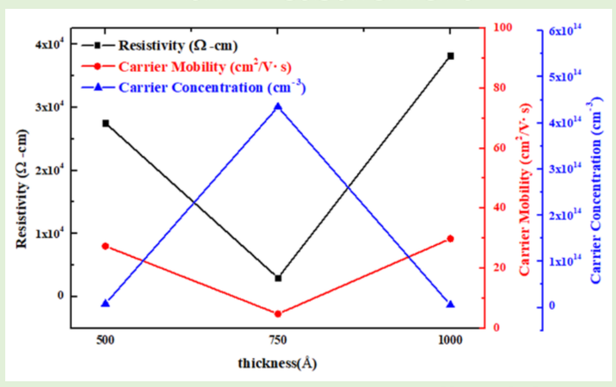

Figure 4. Carrier concentration, Hall mobility and resistivity of ITO films with different film thicknesses annealed at 500˚C.

FOM

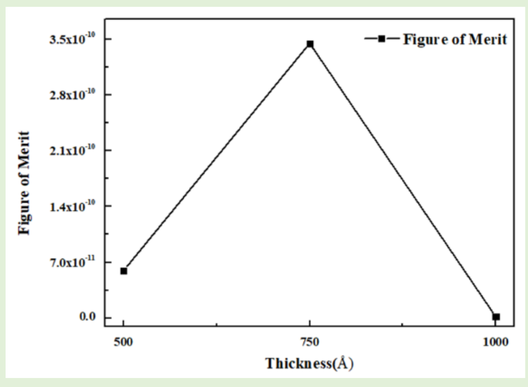

Figure 5. FOM of ITO films with different film thicknesses annealed at 500˚C.

SEM

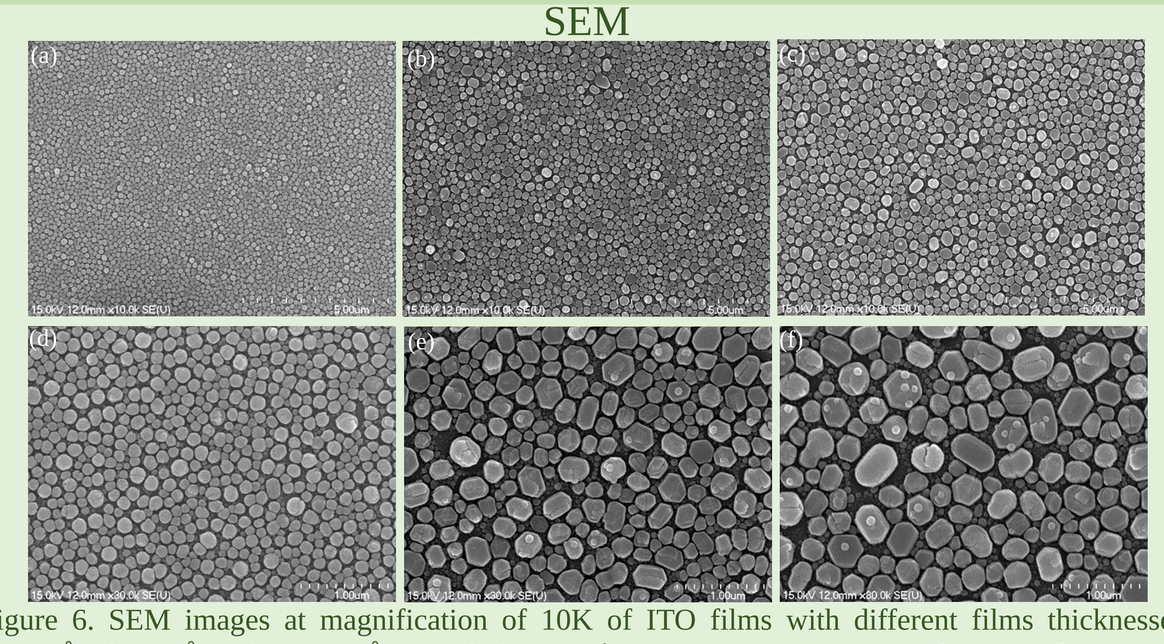

Figure 6. SEM images at magnification of 10K of ITO films with different films thicknesses: (a)500Å, (b)750Å and (c)1000Å annealed at 500˚C. SEM images at magnification of 30K with different films thicknesses: (d)500Å, (e)750Å and (f)1000Å.

Cu_2O films (p-type)

Experimental

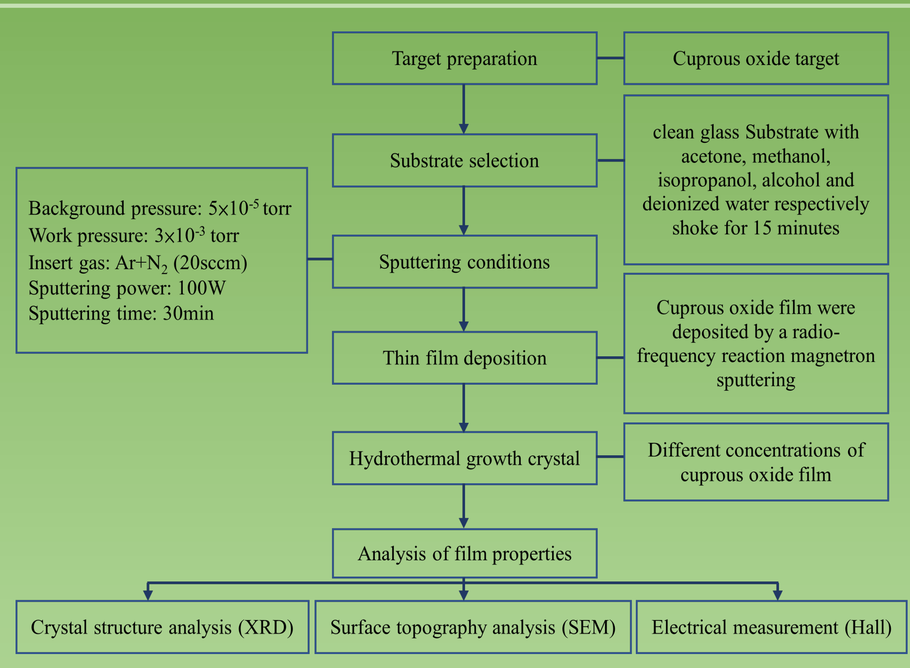

Figure 7. Experimental process of Cu_2O films. Grown on Cu_2O buffer layers on glass substrate by a radio-frequency reaction magnetron, then at 90℃ with hydrothermal time of 6 hours, that have different precursor concentrations from 0.2M to 0.5M deposited films in hydrothermal method.

Results and Discussion

XRD

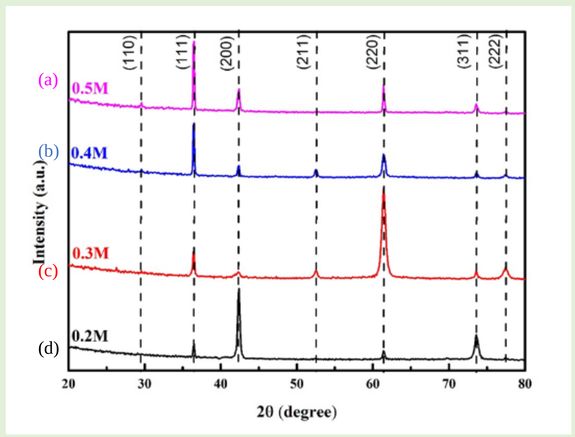

Figure 8. XRD pattern of different precursor concentrations: (a)0.5M (b)0.4M (c)0.3M (d)0.2M in hydrothermal method.

Hall Measurement

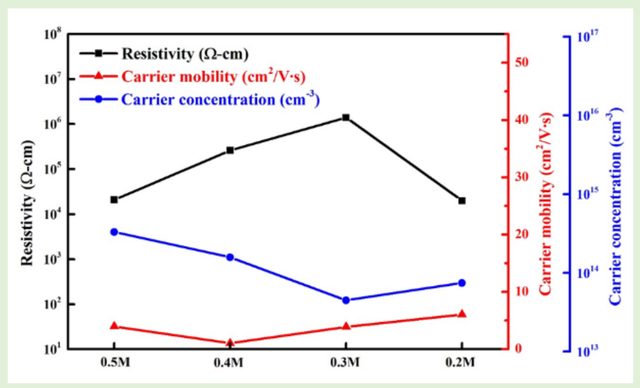

Figure 9. Comparison resisvity properties of Cu_2O flims grown on Cu_2O buffer layers on glass substrate at 90℃ with hydrothermal time of 6 hours.

SEM

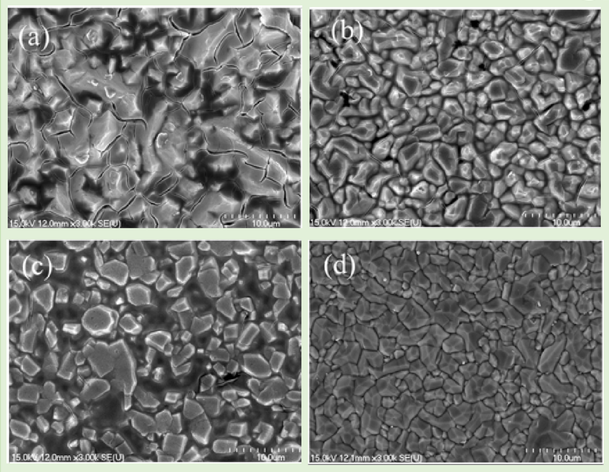

Figure 10. SEM surface structure of Cu_2O flims grown on Cu_2O buffer layers on glass substrate at 90℃ with hydrothermal time of 6 hours, that have different precursor concentrations: (a)0.5M (b)0.4M (c)0.3M and (d)0.2M in hydrothermal method.

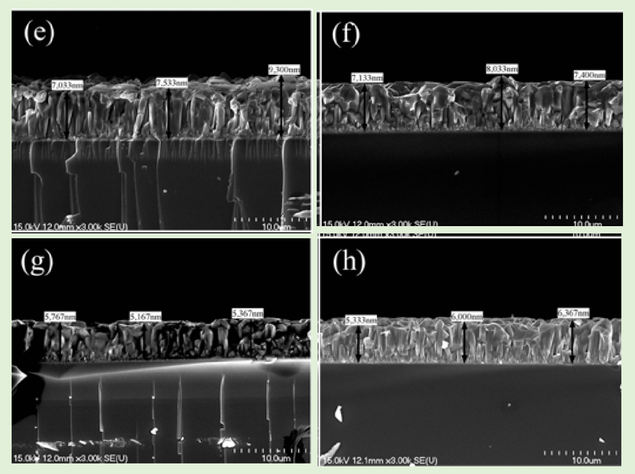

Figure11. SEM cross-section of Cu_2O flims grown on Cu_2O buffer layers glass substrate at 90℃ with hydrothermal time of 6 hours, that have different precursor concentrations: (e)0.5M (f)0.4M (g)0.3M and (h)0.2M.

Conclusions

- ITO films have the best electrical properties at a thickness of 750 Å and an annealing temperature of 500˚C (resistivity is 2.99×10^{3}Ω-cm, Carrier mobility is 4.8cm^2/Vs, carrier concentration is 4.35×10^{14}cm^{-3}, photoelectric quality factor is $3.45\times10^{-10}\Omega^{-1}$.
- Cu_2O films at precursor concentration of 0.2M have the best electrical properties (Resistivity is 2.00×10^{4}Ω-cm, Carrier concentration is 7.45×10^{13}cm^{-3}), and have flat surface suitable for optoelectronic devices. Change the concentration of precursors to obtain thin films with different preferred orientation.

References: [1] G.J. Exarhos and X.D. Zhou, “Discovery-based design of transparent conducting oxide films”, Thin Solid Films, vol.515, 2007, pp.7025.
[2] Andreas Stadler, “Transparent Conducting Oxides—An Up-To-Date Overview ”, licensee MDPI, 2012.

The study on preparation and properties of lanthanide-copper oxysulfide bismuth-doped thin films

Yi-Chi Wang, Hung-Yu Chen, Yi-Ying Tung, Yi-Yang Qiu, Si-Yu Lin, Ji-Yan Luo, You-Wei Zhang, Kai-Ze Gao, Young-Hui Shi, Guo-Ju Chen *
Department of Materials Science and Engineering, I-Shou University, Kaohsiung, Taiwan

In this experiment, the RF magnetron sputtering was used to deposit lanthanum-copper oxides films on the quartz glass substrates. The effects of different bismuth doping concentrations (0at~20at.%) and different sulfidation temperatures on the properties of lanthanumstrontium-copper oxide were discussed. The sulfurization temperature is 600˚C ~800˚C, and the mass of sulfur powder is 2 grams. Sulfur powder is placed near the opening of the tube furnace, the annealing atmosphere is atmospheric argon, and the sulfurization time is 2 hours. The experimental results show that the transmittance and resistivity of the LaCuOS films doped with 10% Bi at a sulfurization temperature of 800˚C are 62% and 1.81 × 10^{-3} Ω-cm, respectively. Meanwhile, FOM of the film (1.07 × $10^{-4}Ω^{-1}$) is the optimal in our study.

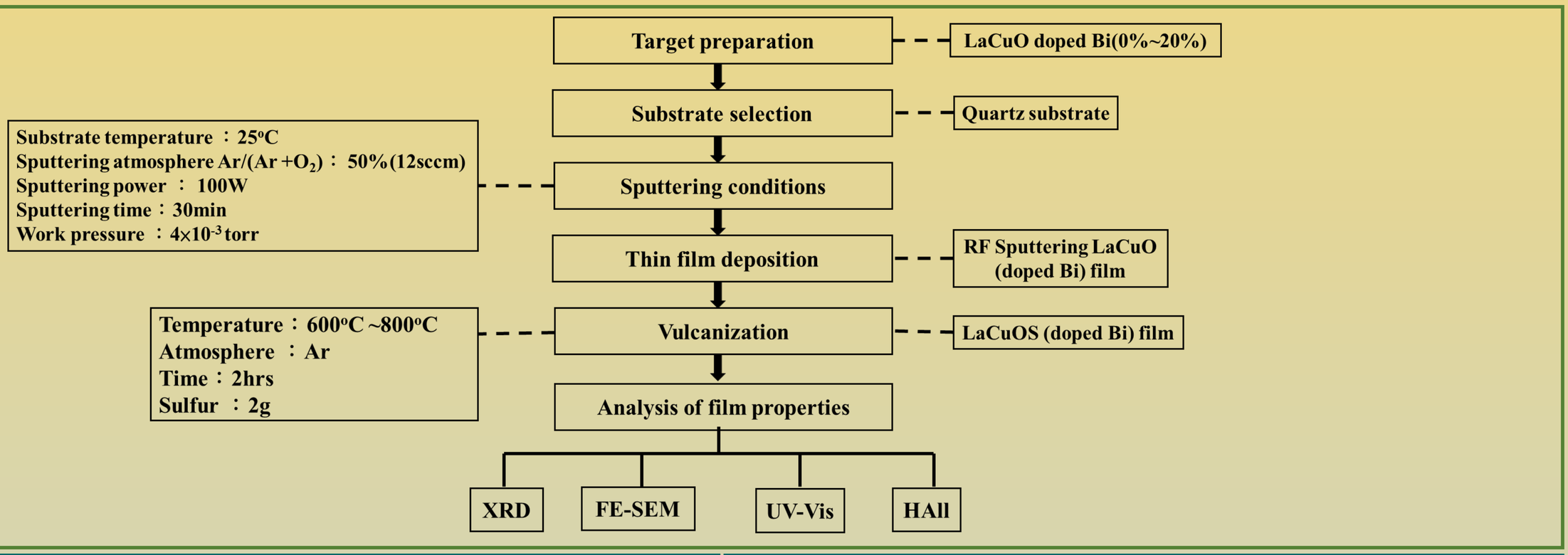

LaCuOS film doped with 10% Bi at different sulfurization temperatures (600~800 ˚C)

SEM

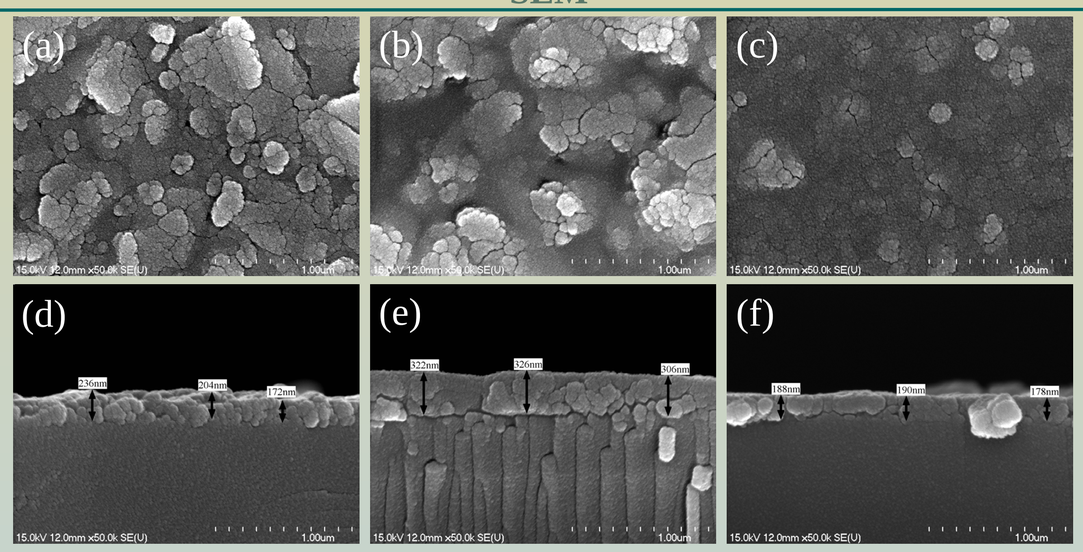

Fig.1 The plane and cross-sectional views of SEM for the LaCuOS films doped with 10% Bi, under different sulfurization temperatures of (a)600˚C, (b)700˚C, (c)800˚C.

Results and Discussion

XRD

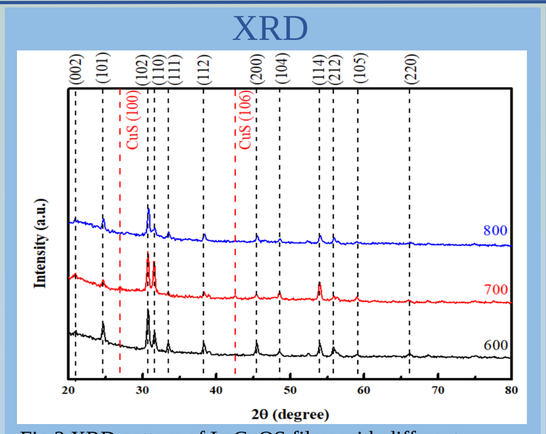

Fig.2 XRD pattern of LaCuOS films with different sulfurization temperatures under 10% Bi doping.

Optical property

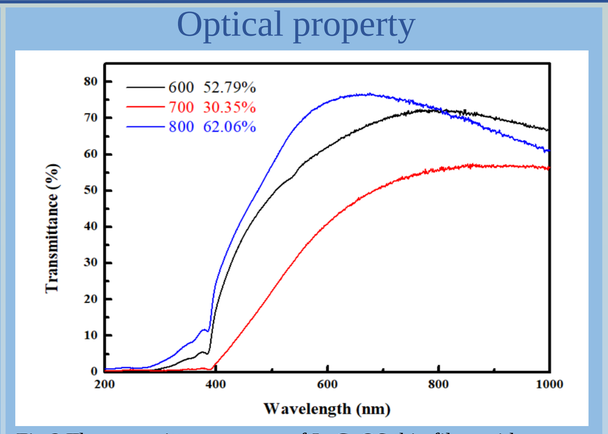

Fig.3 The transmittance curves of LaCuOS thin films with different sulfurization temperatures under 10% Bi doping.

Hall Measurement

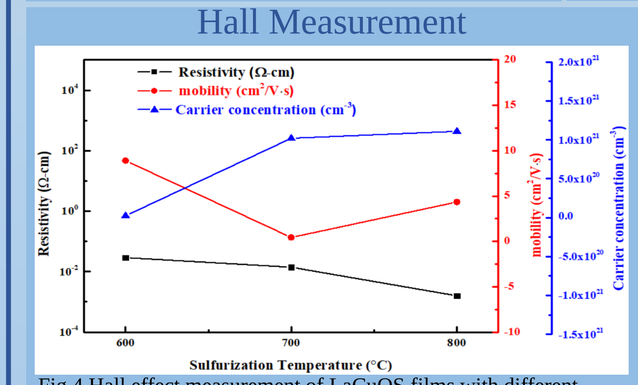

Fig.4 Hall effect measurement of LaCuOS films with different sulfurization temperatures under 10% Bi doping.

FOM

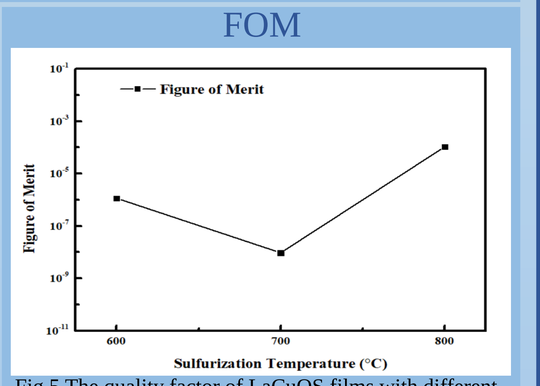

Fig.5 The quality factor of LaCuOS films with different sulfurization temperatures under 10% Bi doping.

0% ~ 20% Bi doped LaCuOS film at temperature of 800˚C sulfurization temperatures

SEM

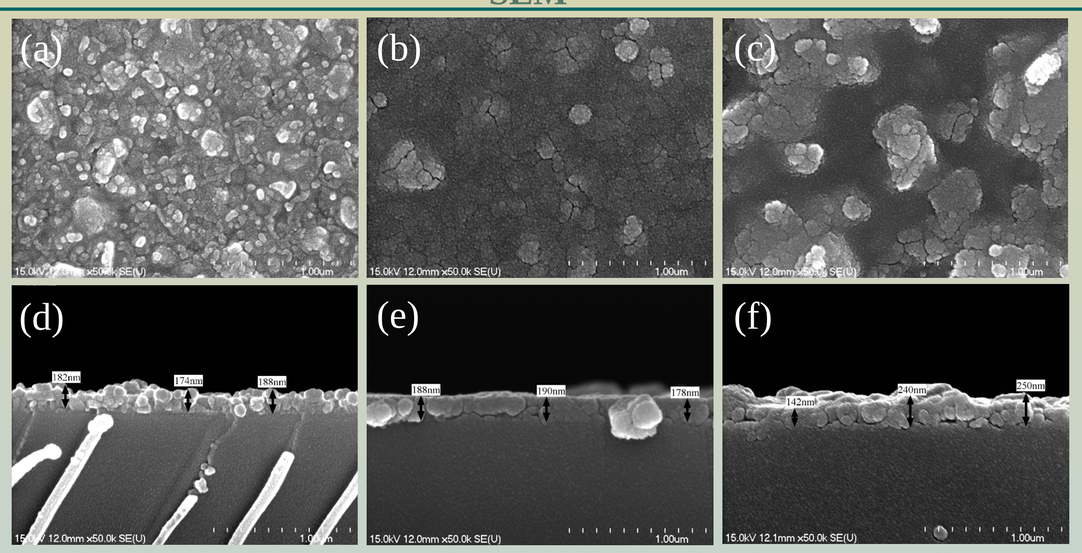

Fig.6 The plane and cross-sectional views of SEM for the LaCuOS films, under sulfurization treatment, with different Bi doping content of (a)0at.%, (b)10at.%, (c)20at.%

Results and Discussion

XRD

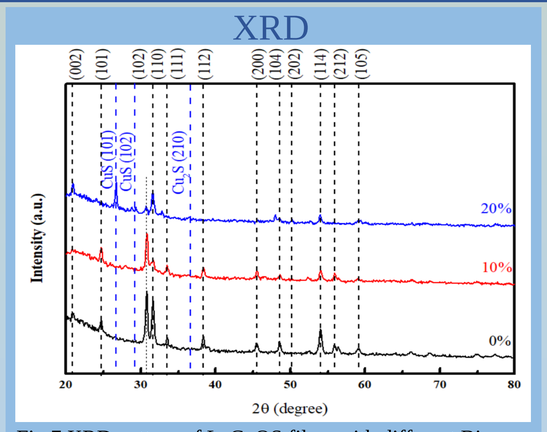

Fig.7 XRD pattern of LaCuOS films with different Bi doping contents (0~20at.%) under sulfurization treatment.

Optical property

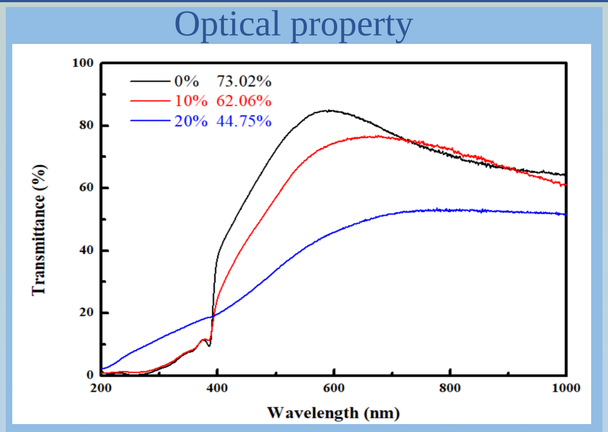

Fig.8 The transmittance curves of LaCuOS thin films, under sulfurization treatment, with different Bi doping (0~20at.%).

Hall Measurement

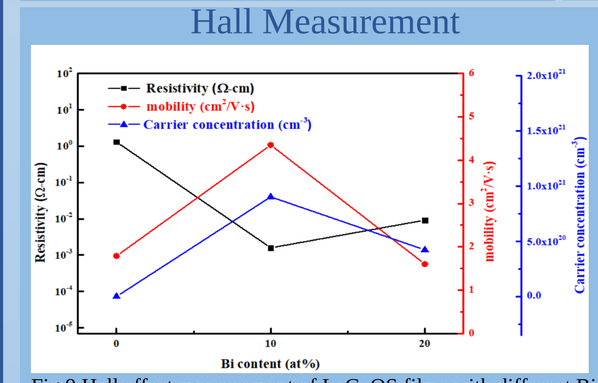

Fig.9 Hall effect measurement of LaCuOS films with different Bi doping content (0~50 at.%), under sulfurization treatment.

FOM

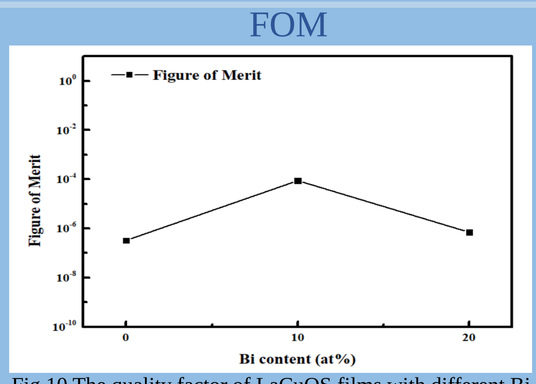

Fig.10 The quality factor of LaCuOS films with different Bi doping contents (0~20at.%), under sulfurization treatment.

conclusions

The experimental results of LaCuOS films with different sulfurization temperatures and different doping levels show that LaCuOS films doped with 10% Bi at a sulfurization temperature of 800˚C have good photoelectric properties with a transmittance of 62.06% and an energy gap of 3.09 eV, the resistivity of 1.81 × 10^{-3} Ω-cm, the carrier mobility of 3.11cm^2/Vs, and the carrier concentration of 1.11 × 10^{21} (cm^{-3}).

Thin films Lab ISU

Persistent Red Emission of $ZnGa_2O_4:Cr^{3+}$ Thin Film Fabricated by Sol-gel Process

Yu-Chien Tseng, Yi-Sin Cheng and Ying-Chi Lin
Advisor: Huy-Zu Cheng
Department of Materials Science and Engineering, I-Shou University, Kaohsiung, Taiwan

Abstract

Cr^{3+} doped $ZnGa_2O_4$ thin film with the composition of $Cr_xZnGa_{2-x}O_4$ were prepared by sol–gel and spin coating method. The crystalline structures of prepared thin film are identified studied by using X-ray diffraction (XRD) and the morphologies are observed by scanning electron microscope (SEM). The photoluminescence (PL) spectra shows that the near-infrared emissions $\lambda_{max.}$ at 694 nm is attributed to ^2E_g-$^4A_{2g}$ transition which reveals that the Cr^{3+} ions are located mainly at octahedral sites. Our result shows that high intensity persistent red emission can be achieved while the pH value of the precursor solution is controlled at 6 and the doping concentration is kept at 2.5 atomic percent .

Experimental Precedure

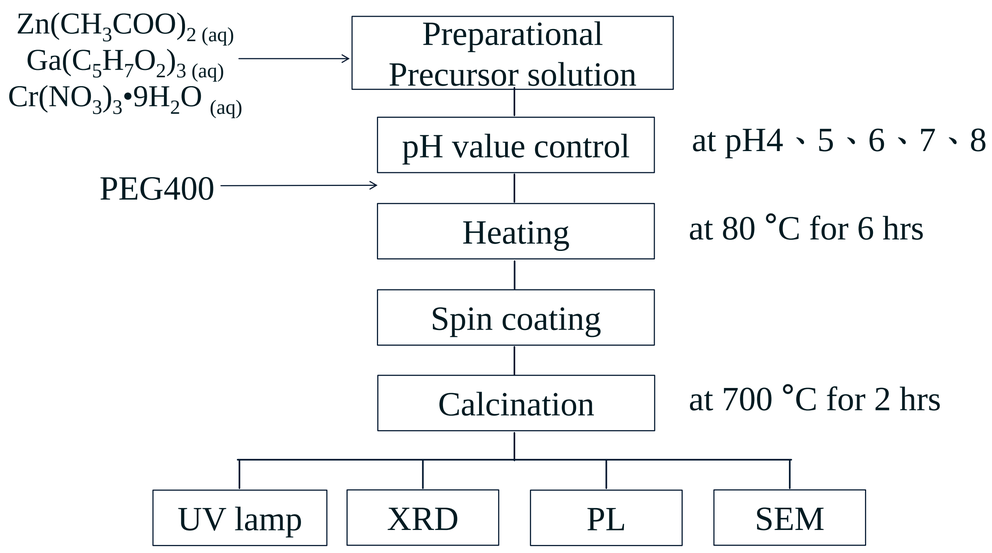

Fig. 1. Experimental procedure

Experimental Results

1. Structure Identification

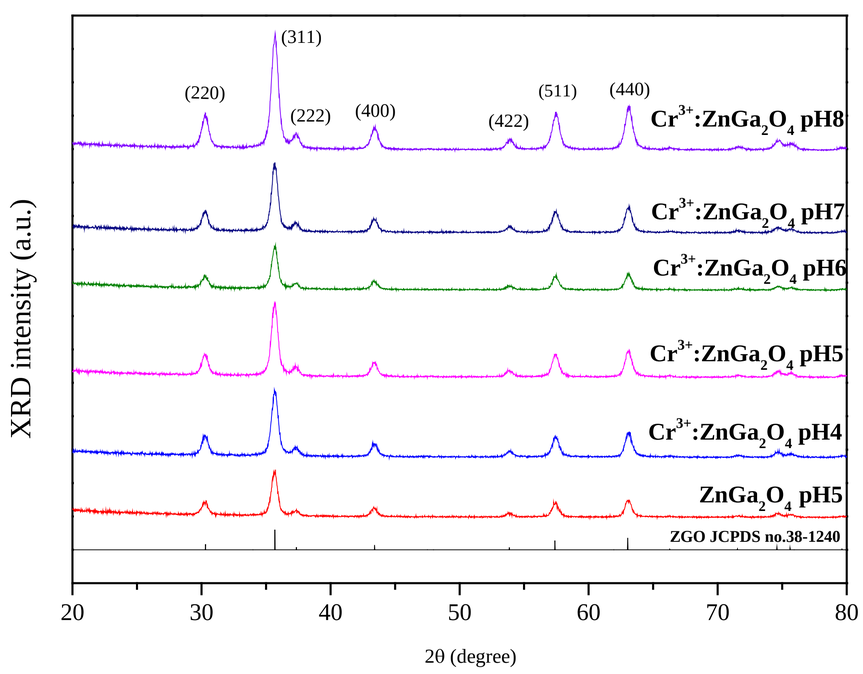

Fig. 2. XRD patterns of 2.5 at % Cr^{3+} doped $ZnGa_2O_4$ thin film changed pH value at 4,5,6,7,8.

2. Emission under UV Lamp

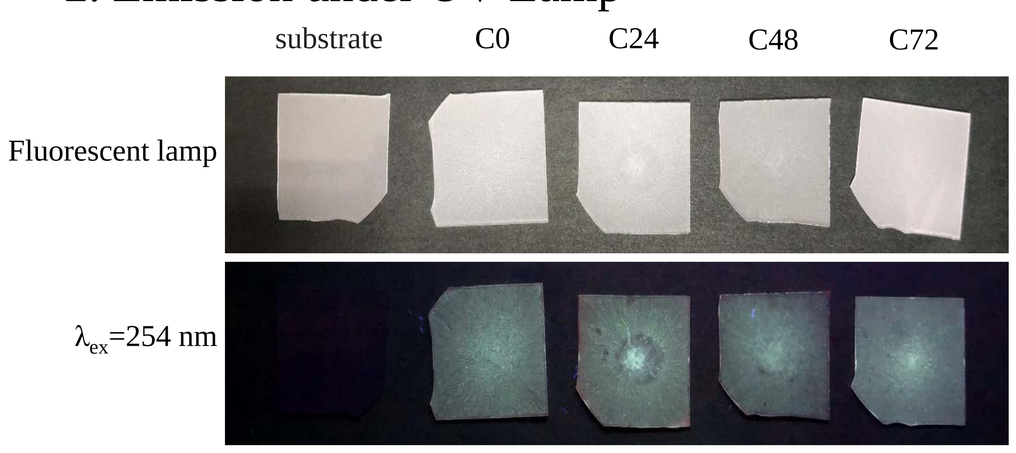

Fig. 3. The as grown $ZnGa_2O_4$ thin film illuminated under fluorescent lamp , UV lamp with wavelength 254 nm and 365 nm at different condensation time for 0 , 24 , 48 , 72 hrs.

3. Morphology Observation

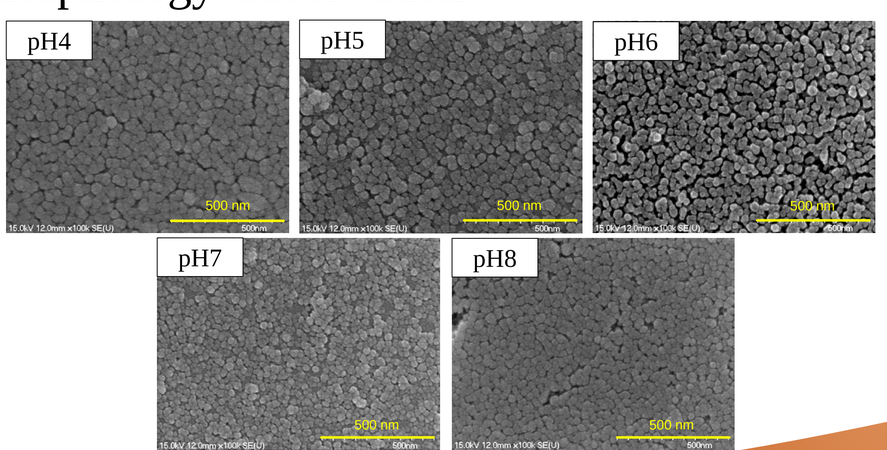

Fig. 4. SEM diagram of 2.5 at % Cr^{3+} doped $ZnGa_2O_4$ thin film changed pH value at 4,5,6,7,8.

4. Photoluminescence Spectroscopy

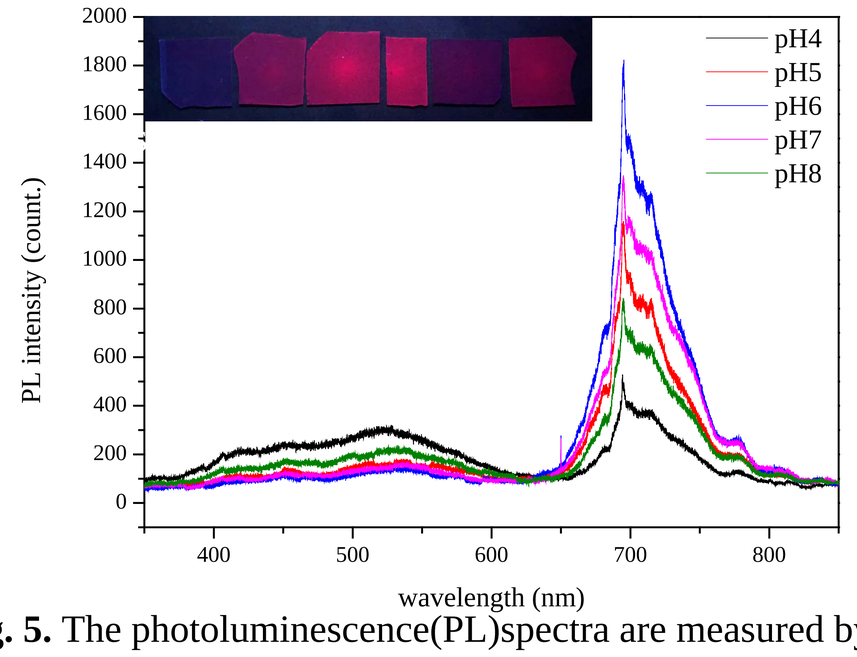

Fig. 5. The photoluminescence(PL)spectra are measured by He-Cd laser excitation with λ=325nm. PL spectra of 2.5 at % Cr^{3+} doped $ZnGa_2O_4$ thin film changed pH value at 4,5,6,7,8.

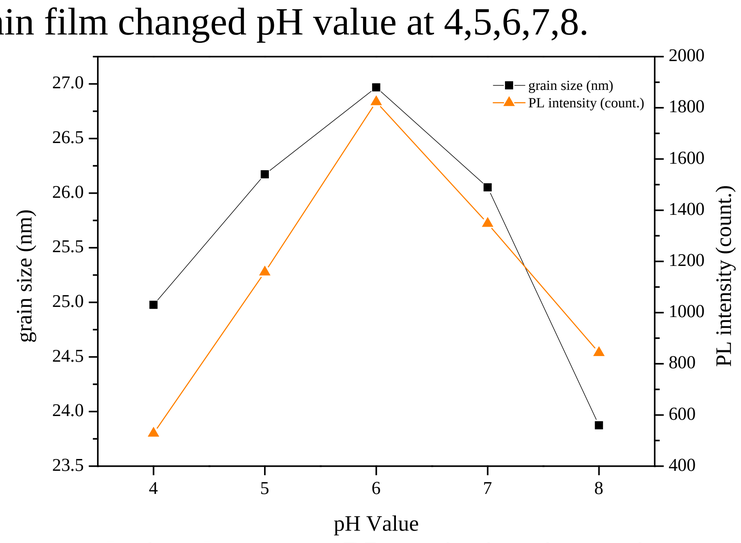

Fig. 6. The correlation between PL emission intensity and the grain size at different pH value.

Experimental Discussion

As shown in **Fig. 1.** Cr^{3+}: $ZnGa_2O_4$ precursor solution was synthesized by sol–gel method using tris(acetylacetonato)gallium(III) and zinc acetate as the reactants. The solution was spin-coated on the C- plane sapphire substrate, and finally calcined at 700 ˚C. **Fig. 2.** is the XRD patterns of $ZnGa_2O_4$ and Cr^{3+}: $ZnGa_2O_4$ thin films synthesized at different pH value. The XRD patterns indicate that no other phases are formed besides $ZnGa_2O_4$. The nanocrystal grain size is about 23–26 nm calculated by Scherrers' equation. It is also found that as the condensation time of the gelation process increases, the uniformity and thickness of the thin film improves as shown in **Fig. 3.**. The morphologies are observed by scanning electron microscope (SEM) as shown in **Fig. 4.** and the diameter of nanocrystals are in nanometer scale. The room temperature PL spectra of Cr^{3+}: $ZnGa_2O_4$ thin-film synthesized at different pH are shown in **Fig. 5.** which show the highest emission at a wavelength of 694 nm. Based on the above results, we found a linear relationship between the grain size and emission intensity while the pH value of precursor solutions is kept lower than 6. However, as the pH value higher than 6, the emission intensity drops as the pH increases as shown in **Fig. 6.**.

Conclusions

1) When the condensation time of sol-gel processes increases, the uniformity and thickness of thin film also increases.
2) The diameter of nanocrystals is strongly related to the pH controlling of precursor solution.
3) pH6 has the highest photoluminescence intensity and largest crystal grain size.

Acknowledgement

The authors are grateful to MOST for the financial support of this study under the Contract No. MOST110-2221-E-214-016 and No. MOST108-2635-E-214-002.

Phosphorescence Fine Tuning of Cations Doped Zinc Gallate Nanocrystals Synthesized by Citrate Sol-Gel Method

Hsin-Tzu, Yu and Jia-Hui, Lin
Advisor : Huy-Zu, Cheng
Department of Materials Science and Engineering, I-Shou University, Kaohsiung, Taiwan

Abstract

Cations doped $ZnGa_2O_4$ (ZGO) nanocrystals were prepared by citrate sol–gel method. The crystalline structures of prepared nanoparticles are identified by X-ray diffraction (XRD). Our results show that the diameters of nanocrystals (NCs) are 20~48 nm after calcination at 700 ℃ or above for 2 hours and the NCs' size increases as the calcination temperature increases. The photoluminescence (PL) spectra shows that Mn^{2+} doped ZGO with λ_{max} at 508 nm is attributed to $^4T_1 \rightarrow {}^6A_1$ transition. Besides, the near-infrared emissions λ_{max} at 694 nm is attributed to $^2E_g \rightarrow {}^4A_{2g}$ transition. This results reveals that the Mn^{2+} ions are located mainly at the tetrahedral sites and the Cr^{3+} ions are located mainly at the octahedral sites.

Experimental

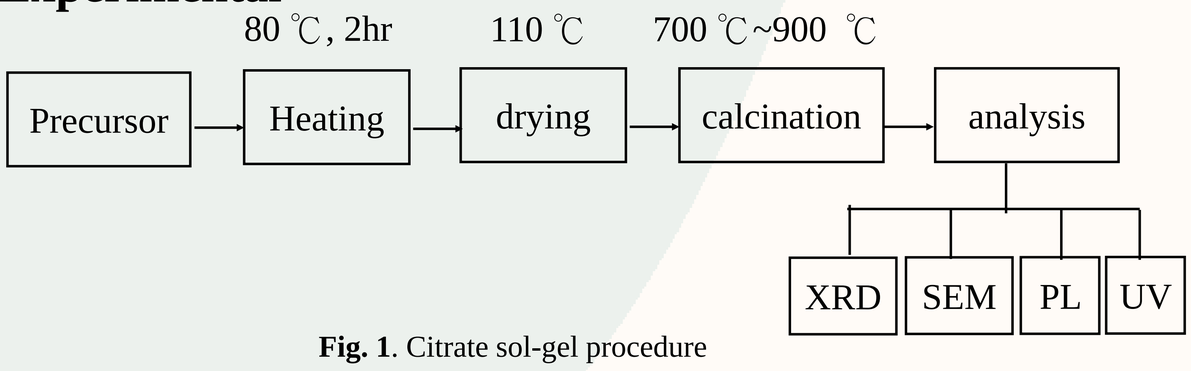

Fig. 1. Citrate sol-gel procedure

Results and Discussions

SEM for Morphology Analysis

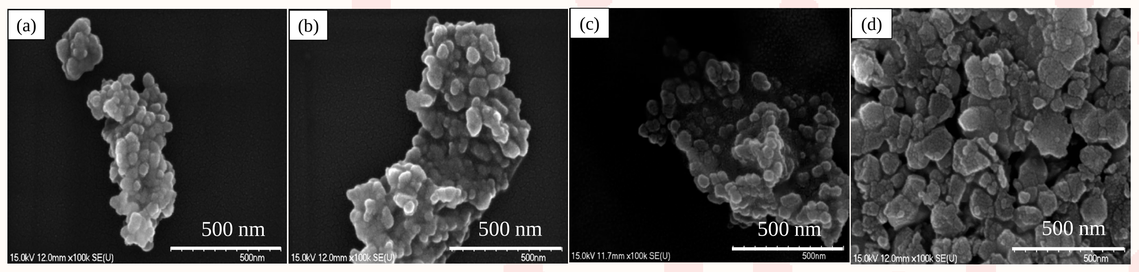

Fig. 2. SEM diagram of $ZnGa_2O_4$ nanocrystals (a) undoped, (b) Mn^{2+}:ZGO, 1 at %, 700 ºC (c) Cr^{3+}:ZGO, 1 at %, 700 ºC, (d) Cr^{3+}:ZGO, 1 at %, 900 ºC

The SEM micrographs in Fig. 2. reveals that NCs' morphologies are almost micro-spherical. Besides, as the calcination temperature increases the size of nanocrystals of ZGO and ZnO increases and aggregates together which may allow defects within the NCs.

Structure Identification by XRD

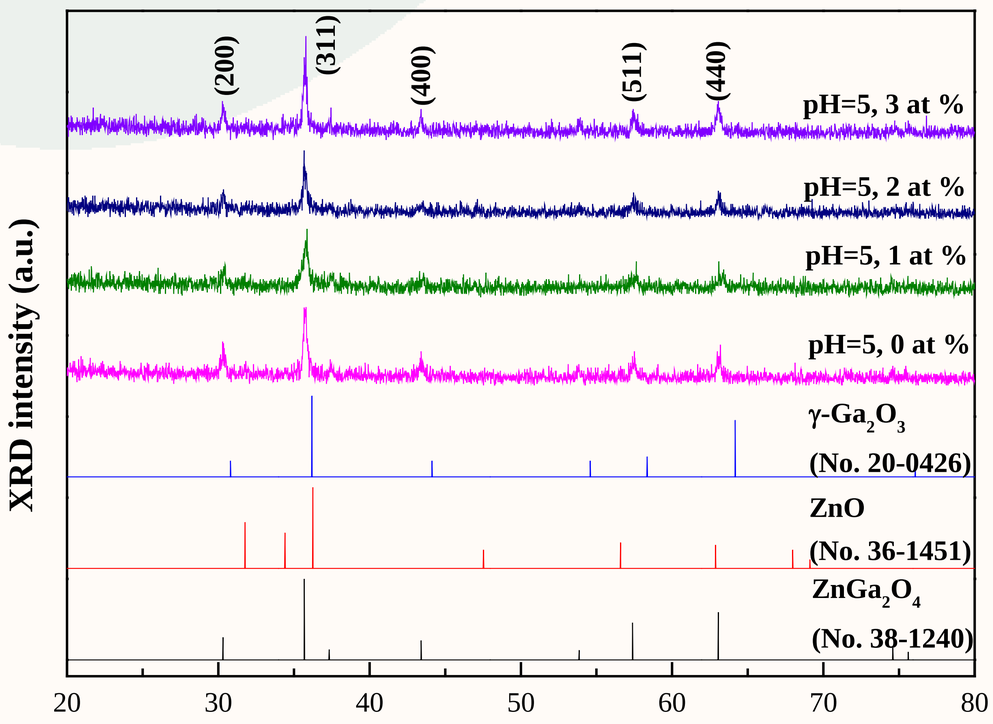

Fig. 3. XRD patterns of 1 at % Mn^{2+} doped $ZnGa_2O_4$ nanocrystals calcined at temperature of 700 ℃.

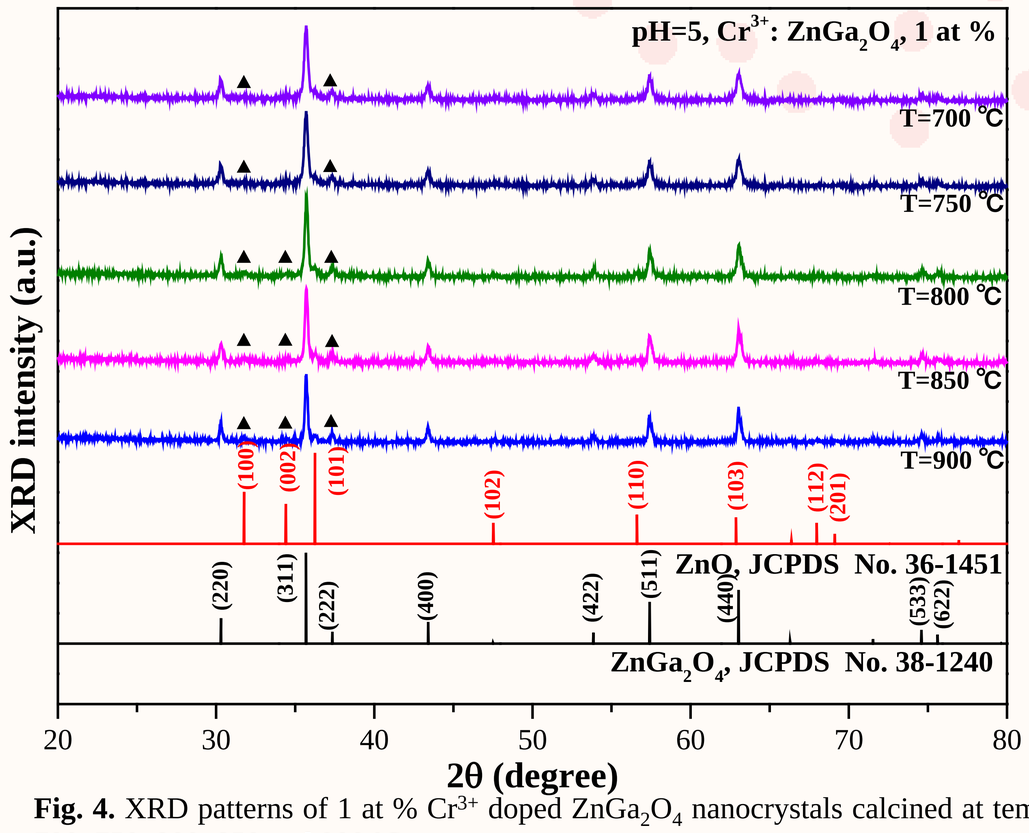

Fig. 4. XRD patterns of 1 at % Cr^{3+} doped $ZnGa_2O_4$ nanocrystals calcined at temperature of 700, 750, 800, 850,and 900 ºC.

Under UV Lamp Observation & PL Analysis

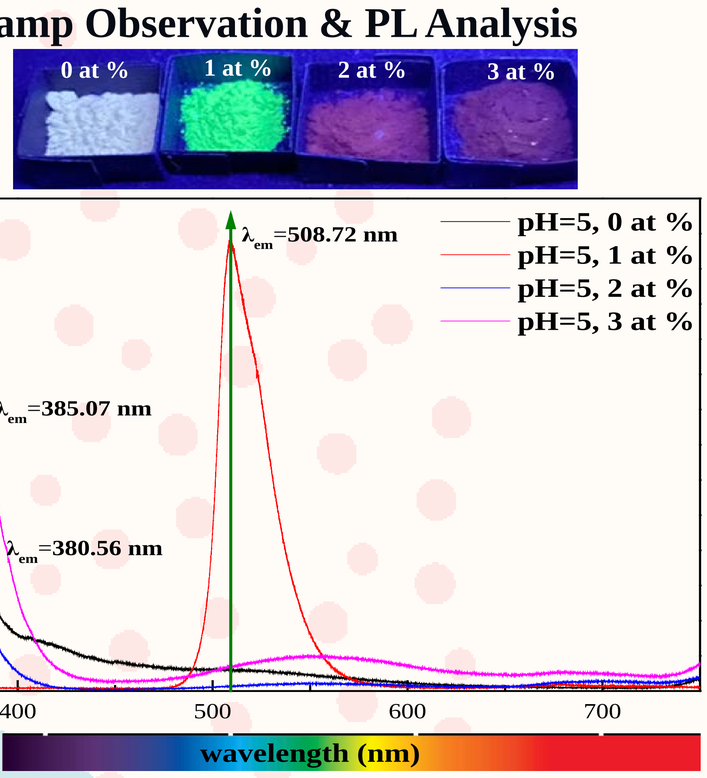

Fig. 5. Above picture shows grown 0~3 at % Mn^{2+} doped $ZnGa_2O_4$ NCs illuminated under UV lamp with wavelength 254 nm and below picture shows the photoluminescence (PL) spectra are of 1 at % Mn^{2+} doped $ZnGa_2O_4$ nanocrystals calcined at temperature of 700 ºC.

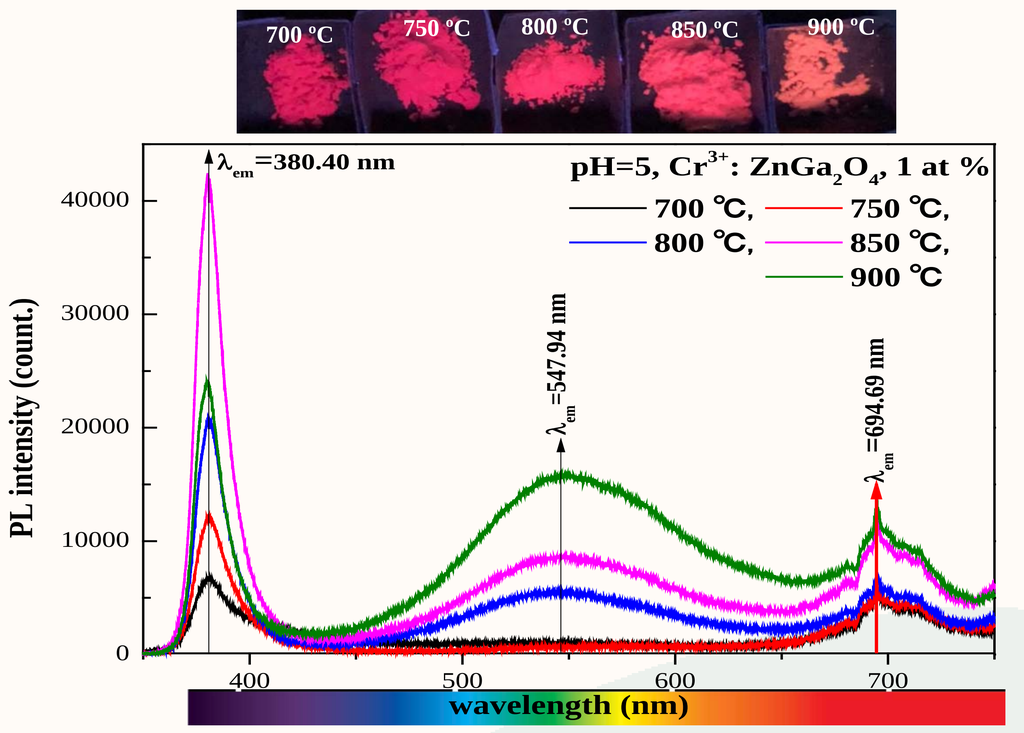

Fig. 6. Above picture shows 1 at % Cr^{3+} doped $ZnGa_2O_4$ NPs illuminated under UV lamp with wavelength 254 nm and below picture shows the photoluminescence (PL) spectra are excitation with λ=325 nm at 700, 750, 800, 850, 900 ºC.

As the results in Fig. 3. the synthesized Mn doped gallate were then identified with XRD. We found the JCPDS card of ZGO, ZnO, and Ga_2O_3. By XRD pattern, we check these nanoparticles are ZGO structure. In Fig. 4. shows by carefully examination of the XRD patterns, a tiny amount of zinc oxide was generated accompany with the production of zinc gallate. The zinc oxide (101) phases as indicated by ▲ in the figure. As the result shown in Fig. 5. we saw green emission under UV lamp with wavelength 254 nm, and according PL spectra, when ZGO doped 1 at % Mn^{2+} under pH=5, green emission is found at λ_{em}= 508 nm. . The unusual intense green emission could possibly result from the oxygen vacancy of zinc oxide. Due to the green emission the Cr^{3+} doped Zinc gallate NCs emit orange light as shown in Fig. 6.

Conclusions

1. According to PL spectra, when ZGO doped 1 at % Mn^{2+} under pH=5, green emission is found at λ_{em}= 508 nm.
2. The ZGO doped 1 at % Cr^{3+} under pH=5 at 750 ℃, there is purely red emission.
3. Zinc oxide phase with very little amount while the NCs calcined at temperature higher than 800 ℃ with Cr^{3+} doping.
4. This enhancement in oxygen vacancy provides one to tune the color of emission light.

Acknowledgement

The authors are grateful to MOST for the financial support of this study under the Contract No. MOST108-2635-E-214-002 & MOST110-2813-C-214-042-E.

以分子動力學模擬碳化矽奈米管在單軸壓縮下之挫曲行為

吳冠勳 簡賸瑞 羅元甫 黃柏瑜 王聖銘

義守大學材料科學與工程學系

一.摘 要

本文以分子動力學方法研究碳化矽奈米管受到軸向壓力所產生的挫曲變形型態與機械性質，主要分析不同管徑尺寸對奈米管挫曲性質的影響及單層奈米管挫曲行為，並使用 Tersoff 勢能函數來描述原子間的互相作用力。

研究結果顯示，楊氏模數及降伏強度會隨奈米管徑越細而下降，而管徑不變為單層奈米管時，楊氏模數會隨直徑越大而下降，降伏強度及挫曲時的應變量在直徑 2.16nm 及 2.48nm 有上升趨勢且挫曲型態為圓柱型挫曲，然而在直徑 3.4nm 之後為下降趨勢其挫曲型態為殼牆型挫曲。

二. 模擬步驟

基本假設 → 模型建立 → 模型參數設定 → 平衡程序 → 後處理

- 模型設計

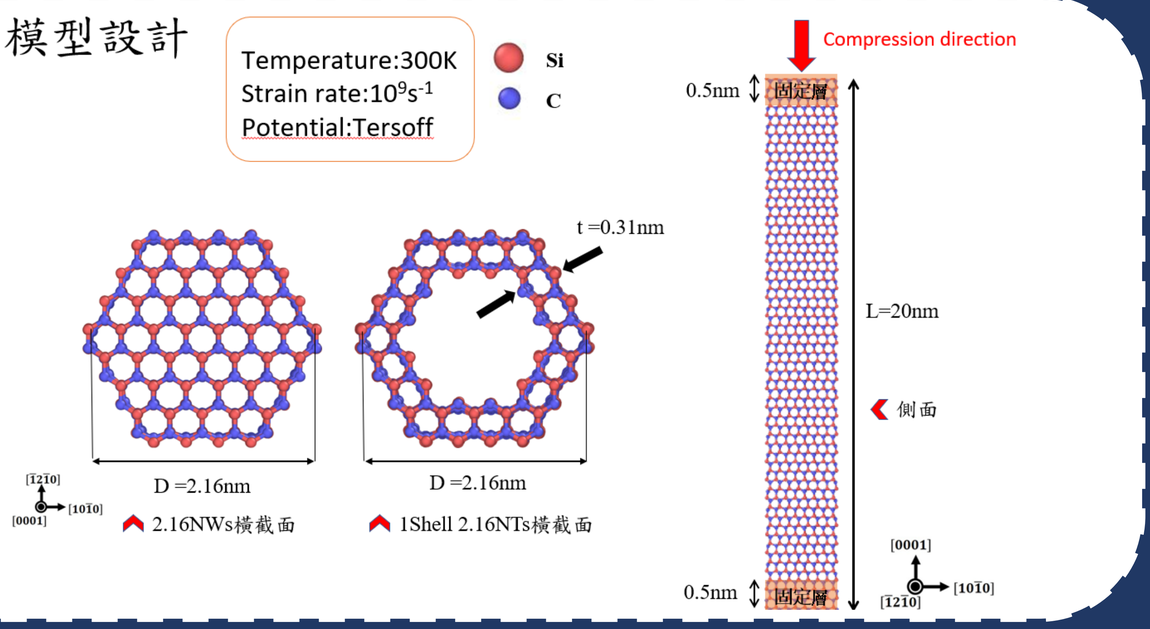

三. 結果與討論

- 管壁效應

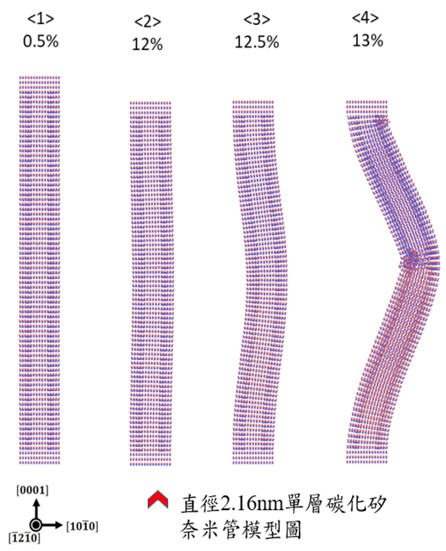

直徑2.16nm單層碳化矽奈米管模型圖

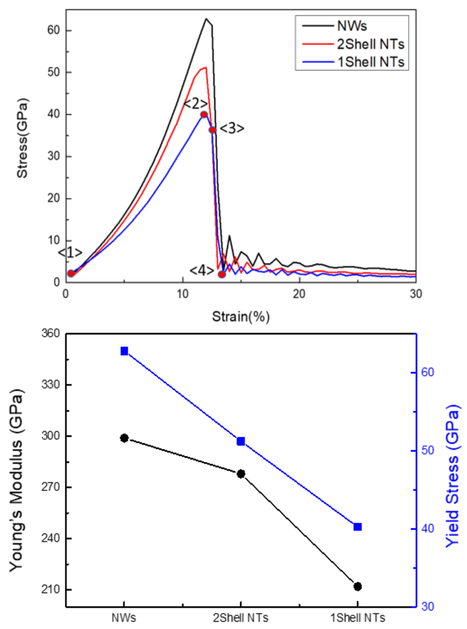

- 直徑效應

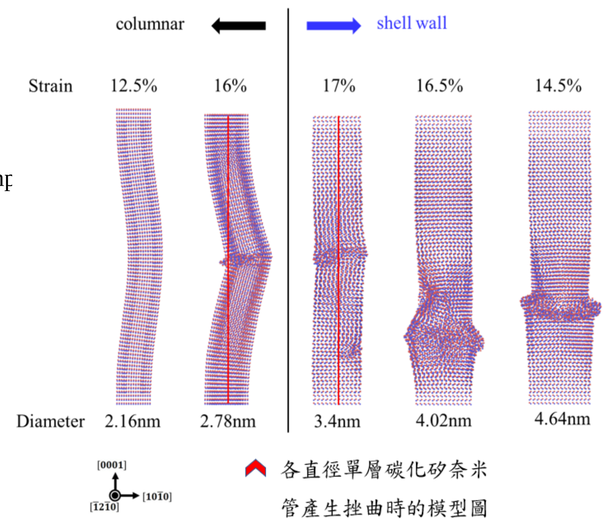

各直徑單層碳化矽奈米管產生挫曲時的模型圖

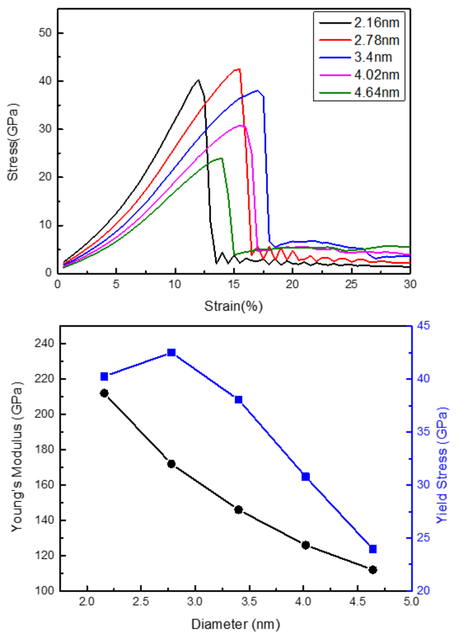

四. 結論

管壁效應

- 管壁越小時楊氏模數以及降伏強度會逐漸下降。
- 管壁的大小並不影響挫曲臨界應變。

直徑效應

- 若直徑越大，楊氏模數會逐漸下降。
- D < 2.78nm時降伏強度及挫曲臨界應變是上升趨勢，
- D > 2.78nm時降伏強度及挫曲臨界應變是下降趨勢。
- 直徑2.16nm ~ 2.78nm為圓柱型挫曲，
- 直徑3.40nm ~ 4.64nm為殼牆型挫曲。